FACULDADE DE ENGENHARIA DA UNIVERSIDADE DO PORTO

Robust Iris Recognition under Unconstrained Settings

João Carlos de Sousa Monteiro

Mestrado Integrado em Bioengenharia

Supervisor: Jaime S. Cardoso (PhD)

Second Supervisor: Ana F. Sequeira (MSc)

August 1, 2012

Robust Iris Recognition under Unconstrained Settings

João Carlos de Sousa Monteiro

Mestrado Integrado em Bioengenharia

Approved by . . . :

President: Pedro Lopes Granja
Referee: Paulo Lobato Correira

August 1, 2012

Resumo

Nos últimos anos, diversos autores têm vindo a reconhecer que o caminho a seguir, relativamente ao reconhecimento da íris, prende-se com o desenvolvimento de algoritmos capazes de ultrapassar as condições em que as imagens são adquiridas, funcionando independentemente destas. Apesar de alguns algoritmos para reconhecimento da íris terem já sido publicados, com taxas de precisão excelentes, trabalhos recentes têm tentado alcançar reconhecimento robusto e não controlado da íris, de forma a desenvolver métodos para aplicações de uso corrente, como sistemas de segurança em aeroportos ou controlo de transferências bancárias por telemóvel. No seguimento desta ideia é necessário o desenvolvimento de novos algoritmos que ultrapassem as limitaçoes existentes aquando da utilização de imagens adquiridas em condições não favoraveis.

Neste trabalho é proposto um novo algoritmo de segmentação e reconhecimento da iris baseado em divergência de gradiente, em conceitos teóricos de grafos e em descritores de pontos de interesse SURF. Informação de contexto mútuo, incluindo a divergência do gradiente, a forma do contorno límbico e intensidade do gradiente ao longo deste, atuam conjuntamente, de forma a detetar o melhor par centro/contorno de um conjunto de candidatos. O reconhecimento foi efectuado extraindo descritores de pontos de interesse utilizando o algoritmo Speeded Up Robust Features (SURF) e calculando os erros de matching entre os melhores pares de pontos de interesse de duas imagens.

O método proposto foi avaliado, inicialmente, na base de dados UBIRISv2, com um erro médio de segmentação de 5.72% e um erro máximo de 14.74% (valores normalizados em relação ao raio da íris). Com o objetivo de tentar desenvolver algoritmos com boa performance de reconhecimento para utilização em dispositivos móveis, uma nova base de dados (VCMI - Visual Computing and Machine Intelligence) foi criada, utilizando imagens adquiridas recorrendo a uma câmara digital convencional e a um *smartphone* Nokia. Com estas imagens, os resultados de segmentação mostraram ser um pouco Com estas imagens, os resultados de segmentação mostraram ser um pouco piores quando comparados com os obtidos para a base de dados UBIRISv2, com um erro médio de 8.18% e de 12.07% para o smartphone e a câmara fotográfica, respectivamente. Contudo, as im- agens da base de dados VCMI apresentaram valores de equal error rate (EER) de 5.56% e 9.35% , valores significativamente menores quando comparados com as imagens da UBIRISv2 (39.2%). Esta discrepância pode dever-se quer à falta de detalhe das imagens da base de dados UBIRSv2, quer à incapacidade do algoritmo desenvolvido quando exposto a imagens de resolução menor. O desenvolvimento de novas métricas de dissimilaridade poderá levar a uma melhoria significativa nos resultados propostos.

Abstract

In recent years many authors have recognized that the path forward, regarding biometrics and iris recognition in particular, is the development of iris recognition systems that can work independently of the conditions under which iris images are acquired. Even though several algorithms for iris recognition are already published, with excellent accuracy rates, recent works are trying to achieve robust and unconstrained iris recognition in order to develop real-world applicable methods, such as security in airports or bank account management through mobile devices, for example. With that in mind new algorithms are needed that can overcome the limitations posed by working with images acquired under non-ideal conditions.

In the present work a new iris segmentation and recognition algorithm based on gradient flow, theoretical graph concepts and SURF point of interest descriptors is proposed. Mutual context information from iris center probability, limbic contour shape and gradient intensity work together to detect the best center/contour pair from a set of candidates. Recognition was performed by extracting point of interest descriptor vectors using the Speeded Up Robust Features (SURF) algorithm and computing the matching error between the best point of interest matches between two images.

The proposed methodology was evaluated initially in the UBIRISv2 database, with a 5.72% mean and 14.74% maximum segmentation error, with respect to the radius of the iris. With the goal of analyzing the applicability of the proposed algorithm in images acquired with mobile devices, a new unconstrained iris database, the VCMI (Visual Computing and Machine Intelligence) database, was created using simple portable devices, such as a smartphone and a standard digital consumer camera. With such images the segmentation results were slightly worse than for the UBIRISv2 images, with mean errors of 8.18% and 12.07% for the smartphone and digital camera images respectively. However, the VCMI images presented equal error rate (EER) values of 5.56% and 9.35%, which were both significantly lower than the value obtained for the UBIRISv2 images (39.2%). These discrepancies might indicate either a limitation of the UBIRISv2 database, as far as recognition algorithm evaluation is concerned, or a limitation concerning the minimum resolution under which the proposed algorithm works correctly. The development of new similarity metrics might lead to a significant improve on the present results.

Agradecimentos

Este trabalho não teria sido possível sem a contribuição de variadas pessoas e entidades, às quais dirijo, desde já, o meu mais sincero obrigado: ao Professor Jaime Cardoso, por todo o acompanhamento, orientação, e o ocasional (sempre saudável) raspanete; ao INESC TEC e, em especial, ao grupo VCMI (Visual Computing and Machine Intelligence), por me terem fornecido o ambiente ideal para o trabalho desenvolvido; em especial à Ana Filipa Sequeira e ao Hélder Oliveira (sem ordem especial) por me terem acompanhado mais de perto, por me suportarem sempre que necessário e por não hesitarem em me repreender sempre que merecido. Sem vocês nada disto seria sequer remotamente imaginável!

Mas, há pessoas ainda mais importantes, que me fizeram chegar aqui, a esta sala da Rua Augusto Lessa, onde me encontro a escrever este parágrafo. Sem elas não seria a pessoa que sou hoje e, por arrastamento, tudo o que consegui neste curso é devido a elas. Poderia começar pelo cliché de agradecer aos meus pais, mas eles sabem que não seria nada meu fazê-lo. E também sabem que não é necessário. À Rita Moreira, por todas as (muitas e penosas) horas em que me aturou durante este ano, por todo o apoio (às vezes até em demasia), confiança (cega e absoluta), e paciência (do tamanho do mundo) com que soube lidar com a minha difícil personalidade. Prometi-lhe um parágrafo só para ela mas seria complicado expressar tudo em tão poucas linhas portanto acho que me vou calar. Aos que comigo entraram na faculdade e me acompanharam neste 5 anos de aventuras e desventuras, noites de borga e estudo, dias intermináveis, noites inesquecíveis. Podia listá-los mas, mais uma vez, o espaço não é suficiente para tão grandes pessoas. A 2007/08 o maior dos obrigados. À Praxe, por ser exatamente o contrário do que todos pensam, por ter pegado num pirralho irritante e arrogante, e o ter transformado num rapaz um pouco mais crescido, irritante e arrogante na mesma, mas respeitador, trabalhador, empenhado, a perder noites pelo bem de uma causa maior, pelo orgulho, pela tradição, por uma causa, por um curso. E para evitar ciúmes e quezilias entre todos os que comigo partilharam frações, mais ou menos elevadas, do tempo que passei neste curso, um agradecimento breve mas pleno de sentimento (e o tradicional abraço claro) para 2008/09, 2009/2010, 2010/2011 e 2011/2012 (sem nenhuma ordem específica, como é óbvio). Por me terem sobrevivido devo-vos isto.

Muitos terão ficado de fora, eles saberão, eu saberei quando a sua ira recair sobre mim. Mas para me resguardar um agradecimento aos ausentes sempre presentes dos meus agradecimentos. Se algum dia me apanharem na rua, por favor encontrem dentro de vós a piedade de perdoarem a minha falta de atenção.

João Carlos Monteiro

“Every day is a new day. It is better to be lucky. But I would rather be exact. Then when luck comes you are ready.”

Ernest Hemingway, “The Old Man and the Sea”

Contents

List of Figures

List of Tables

List of acronyms

FAR	False Accept Rate
FN	False Negative
FP	False Positive
FRR	False Reject Rate
ROC	Receiver Operating Characteristic
SURF	Speeded Up Robust Features
TAR	True Accept Rate
TN	True Negative
TP	True Positive
VCMI	Visual Computing and Machine Intelligence

Chapter 1

Introduction

1.1 Overview

The accurate recognition of an individual, from a given set of possibilities, represents a critical issue in many areas, especially concerning security. The development of reliable and robust recognition methods has become an increasing challenge over time, due to limitations inherent to such systems. The use of an identifying item (magnetic card, password, etc.) is still, as of today, the most widespread method of identification. It is not complicated, however, to imagine the relative ease with which a system based on these prerogatives may be deceived: the password can be acquired from the person who would, ideally, be the only one to know it; one card can be lost and found by another person, etc. Thus the paradigm of personal recognition has shifted from the use of something that person has to something a person is. This is where biometrics, the methods for uniquely recognizing humans based on physical and behavioral characteristics of living things (Jain et al., 2000) may play an important role.

1.2 Motivation

Several biological traits in humans show a considerable inter-individual variability: fingerprints and palmprints, the shape of the ears, the pattern of the iris, among others. Biometrics works by recognizing patterns within these biological traits, unique to each individual, to increase the reliability of recognition. Among all the biometric variables that are the subject of research nowadays, the iris presents itself as a leading candidate to become the standard biometric trait: the variability is huge, apart from being an organ easily accessible and very difficult to modify. Currently, there are several systems based on iris recognition with excellent rates of success. However, these results are due to the very constrained conditions under which iris data is acquired (IR illumination of the eye, user collaboration, etc.). The new challenges for iris biometric systems arise when the attempt is made to perform iris recognition without user cooperation or under less ideal conditions (subject on the move, natural illumination, distance, etc.). If there was a system capable to work under such unconstrained settings, individuals could be covertly identified, that is, identified without knowing they were being identified. This would represent a huge step forward in security. Some other applications would be a user friendly method for personal verification, something like a biological password, unique for every human, acquirable by a simple smartphone camera for example.

1.3 Objective

The main objective of the present dissertation is the development of robust algorithms for the detection, segmentation and recognition of the human iris in non-ideal conditions. Such algorithm was tested both in the UBIRISv2 database (Proença et al., 2010), developed by Hugo Proenca from Universidade da Beira Interior, and a newly created database developed by the author and some collaborators of the project. One of the proposed objectives was also to test the application of the developed algorithms using images acquired with mobile devices, with possible future mobile recognition applications in mind. As, to our knowledge, no iris database has been developed using only mobile devices, a new iris database, the VCMI database, was created integrated in the present dissertation.

1.4 Contributions

The proposed work had three main contributions: first it suggested a gradient flow based algorithm for iris center detection with a variation of a shortest path algorithm to detect iris contour. Second it used mutual context information from two data sources (iris center and limbic contour) to perform segmentation of the iris. Finally a new iris database was created, using solely mobile devices (smartphone and camera), to analyse the usability of the developed algorithms in such environments. Two papers were produced in the ambit of the present work, with one of them still awaiting review:

- Monteiro, J. C., Oliveira, H. P., Sequeira, A. F., and Cardoso, J. S. (2012). Gradient flow based iris segmentation in noisy images. Paper presented at the 1st PhD Students' Conference in Eletrical and Computer Engineering, Porto, Portugal.

- Monteiro, J. C., Oliveira, H. P., Sequeira, A. F., and Cardoso, J. S. Robust Iris Recognition Under Unconstrained Settings. ISRN Machine Vision (submitted).

1.5 Structure of the Dissertation

Besides the introduction, this dissertation is composed of five more chapters. In chapter 2 a global introduction to the field of biometrics will be presented. In chapter 3 some insight will be provided regarding the use of the human iris for identification. Still in this chapter the pioneer and state-of-the-art algorithms for iris recognition, as well as the most recent trends in the area, will be presented, with major focus on the works for unconstrained iris recognition. Chapter 4 describes the developed algorithm, whose main results are presented in Chapter 5. Finally, chapter 6 serves as a conclusion to the presented dissertation, while presenting a set of future improvements for the developed algorithm.

Chapter 2

Biometrics

2.1 Why Biometrics?

From times immemorial mankind has relied on specific features, such as face or voice, to distinguish between individuals. The term biometrics has evolved through time, as technological breakthroughs made available new and powerful tools, and nowadays it can be defined as the automated measurement of intrinsic biological features of a human being, with the objective of obtaining quantitative values that allow us to, with a high degree of confidence, distinguish between separate individuals (Proença, 2007). The importance of biometrics is strongly related with the rising need of reliable recognition systems with multiple purposes and applications, from security to forensics (Jain et al., 2000). In almost everyone's daily activities, personal identification plays an important role. The most traditional techniques to achieve this goal are knowledge-based and token-based automatic personal identifications. Token-based approaches take advantage of a personal item, such as a passport, driver's license, ID card, credit card or a simple set of keys to distinguish between individuals. Knowledge-based approaches, on the other hand, are based on something the user knows that, theoretically, nobody else has access to. Examples of these systems are passwords or personal identification numbers (PIN). Both of these approaches present obvious disadvantages: tokens may be lost, stolen, forgotten or misplaced, while passwords can easily be forgotten by a valid user or guessed by an unauthorized one (Jain et al., 2000). In fact, all of these approaches stumble upon an obvious problem: any piece of material or knowledge can be fraudulently acquired, making token and knowledge-based identification unsatisfactory means of achieving the security requirements set by our society's needs. Some works put numbers on these disadvantages' consequences: in 1998, Anil Jain's research (Bolle and Pankanti, 1998) indicated that 6 billion dollars were reported lost every year as a result of identity fraud, in some areas where security played a key role: credit-card transaction, cellular phone calls, ATM withdrawals, etc. Biometrics represents a return to a more natural way of identification: many physical or behavioral characteristics are unique between different persons and these markers are inherently more reliable than knowledge-based or token-based techniques. Testing someone by what this someone is, instead of relying on something he owns or knows seems likely to be the way forward: it is clearly more difficult to change a fingerprint or gait pattern than acquiring a physical item or piece of knowledge. Taking advantage of specific unique biometric features to develop robust and reliable identification systems is, therefore, an important challenge for the years to come, to accompany the growth of technological innovation and the security challenges that such growth will undoubtedly carry.

2.2 A brief historical overview

Use of human physical and behavioral patterns for identification is as old as mankind itself. Some paintings in a cave in Avignon, France, dated 31.000 years, and depicting hunting scenes, are accompanied by palm prints (Figure 2.1) that archeologists believe to have been used as some kind of a specific signature by the author (Bala, 2008; Renaghan, 1997). One does not even need to know history to understand that mankind has always relied on faces and voices to distinguish between familiar and unfamiliar individuals. However, if written accounts of biometrics are needed to establish the birth of this science, one must turn to Portuguese writer Joao de Barros, who, in the 14th century, reported its first known application. According to his writings Chinese merchants stamped children's palm and foot prints on paper with identification purposes (Proença, 2007; Bala, 2008).

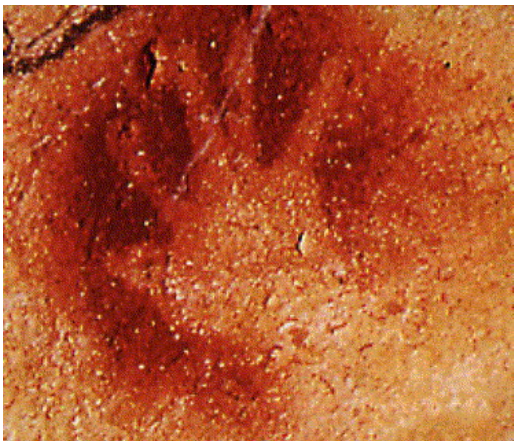

Figure 2.1: Palmprint discovered in a cave in Avignon, France, dated 31.000 years (Barnett et al., 2006).

In the 19th century, the first scientific and systematic method for human identification was created by French anthropologist Alphonse Bertillon who introduced the use of a number of physical measurements to identify usual criminals (Jain and A., 2010; Proença, 2007). This method consisted of identifying people by performing several body measurements such as height, arm length, length and breadth of the head, length of fingers, length of forearms, etc. (Angle et al., 2005). As it can be deduced by the significant number of features, and their schematization in Figure 2.2, this was a very time consuming process, which could take up to twenty minutes per person. This fact,

Figure 2.2: Schematization of some of the measurements performed as part of Bertillon's recognition system (Proença, 2007).

combined with the introduction of human fingerprints early in the 1900s, turned the Bertillonage obsolete, eventually leading to its demise.

In 1880, an article was published in the British scientific journal Nature, where its authors, Henry Faulds and William James, described the unique nature of fingerprints (Proença, 2007). Soon after, Sir Francis Galton developed the first elementary fingerprint recognition system, soon improved by Sir Edward Henry (Figure 2.3) who, for criminal identification purposes, established the fingerprint Bureau in Calcutta in 1897 [8]. The success of Henry's method quickly disseminated throughout the world and led to the inauguration of the first fingerprint system in the United States in 1903 in the New York State Prison (Proença, 2007). From that point onwards fingerprinting grew on to become the standard security biometric system for worldwide. Nowadays, virtually all law enforcement agencies use Automatic Fingerprint Identification System (AFIS) (Jain and A., 2010).

Nevertheless, fingerprints are also facing the risk of becoming an ineffective trait for the purposes they were considered the gold standard for almost a century. With growing concerns about terrorist activities, security breaches and financial fraud, an increasing number of private and governmental companies, with either military or civil purposes, have been investing a considerable amount of human and financial resources in the attempt of developing biometric systems based on

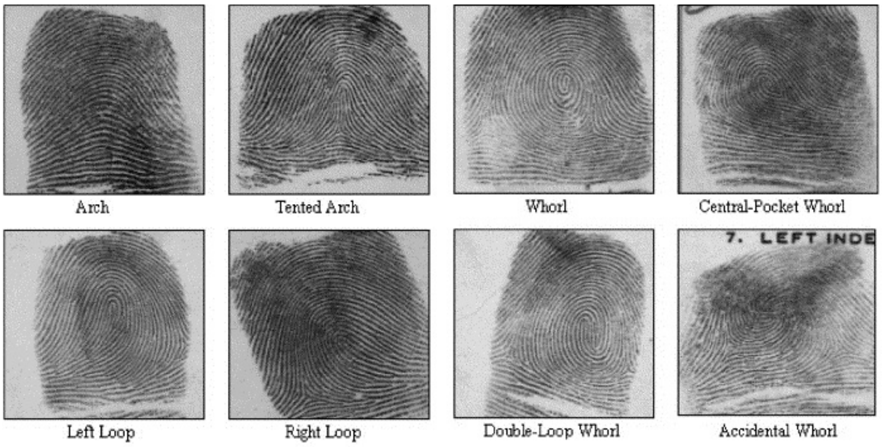

Figure 2.3: Examples of patterns used in Sir Edward Henry's fingerprint classification system (Chang and Fan, 2002).

other physical and behavioral human characteristics such as face, iris, palm print and signature (all of these traits and other will be presented in detail in later sections) (Proença, 2007; Jain and A., 2010). In the last few years biometrics has started to find its way into an incredibly heterogenic group of applications, as contrasting as border crossing or visits to Walt Disney Parks, as it grew to become a mature technology with lots of promise in the years to come (Jain and A., 2010).

2.3 Basic concepts of biometrics

2.3.1 System architecture

A biometric system can be viewed as a pattern recognition system that establishes the authenticity of a user based on specific physical or behavioral traits. All biometrics systems, independently of the chosen trait to serve as its basis, follow a specific process, as schematized in Figure 2.4, which can be divided into two main blocks: enrollment and identification (Jain et al., 2000; Proença, 2007). Enrollment consists in the acquisition of data which is known to belong to a certain individual. In this way a database can be built containing template data concerning a specific group of individuals. Enrollment can, therefore, be simply designated as the registration of a new individual to the database. Identification consists in data capturing and feature extraction to create a specific biometric signature. This signature is compared to the several biometric signatures (exactly how many depends on the mode of operation, as described below), already stored as templates in the database, yielding, for each one, a similarity value. One assumes that two signatures come from the same person if this similarity values exceeds a specific threshold (Proença, 2007). The choice of this threshold value will have the upmost importance in the definition of solid evaluation methods for biometric systems. This topic will be addressed in later sections.

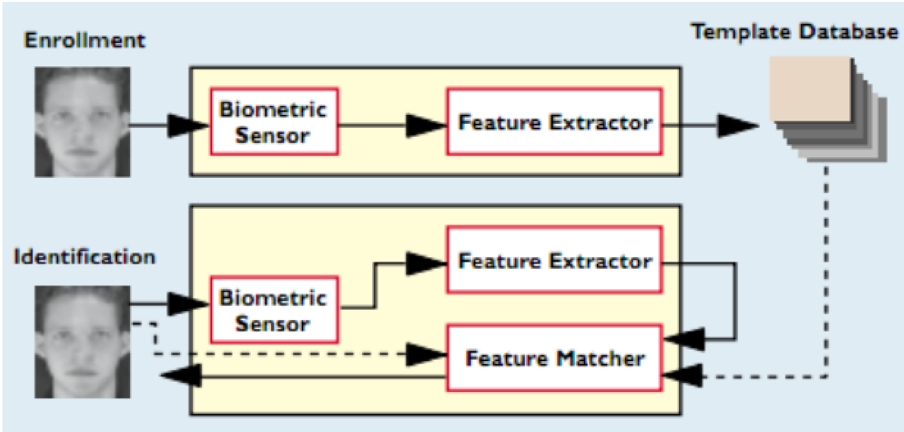

Figure 2.4: Functioning process of a biometric system (Jain et al., 2000).

2.3.2 Operating mode

Depending on the application, a biometric system may operate either in verification or recognition mode (Jain et al., 2000). These two operating modes are depicted in Figure 2.5. A verification system, also known as positive recognition, authenticates a person's identity by comparing captured data with the person's own biometric template. In these cases, an individual claims to be a specific person. This information is passed to the algorithm, which then proceeds to create the biometric signature from the captured data and to compare it to the stored templates whose ID match the claim made by the individual, evaluating the probability that this individual is who he/she claims to be. In a recognition system, one individual's biometric signature is compared to the entire database, with the goal of discerning the subject's ID instead of just proving a claim. In this mode it is usual to present a list of the k most probable identities for the tested individual (Proença, 2007).

2.3.3 System requirements

No biometric system will ever be perfect, in the sense that no system will ever be able to counter all the attempts made to circumvent it, presenting 0 error rate, no matter the conditions. However, with the growing need for reliability and robustness, some expectations started to rise and become the focal points of attention when someone is trying to develop a new system based on a specific trait (Jain et al., 2000):

1. *Universality:* every person must possess their specific variation of the trait.

2. *Uniqueness:* no two persons should share the same specific variation of the trait.

3. *Permanence:* the trait should neither change nor be alterable.

4. *Collectability:* the trait must be readily presentable to a sensor and easily quantifiable.

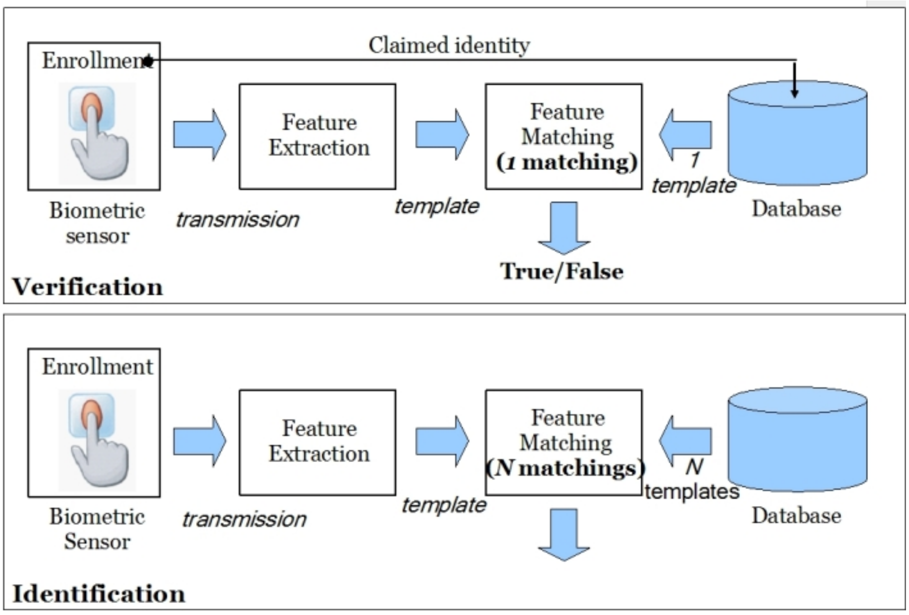

Figure 2.5: Functioning process of a biometric system (Biometrics, 2008).

Regardless of the chosen trait, as long as it follows the four focal points presented above, every biometric system is expected to present some functional requirements that make them acceptable for the tasks they are developed to perform. From a functional point of view one can define some specific requirements that are expected from a biometric system (Jain and A., 2010):

1. *Performance:* a biometric system is prone to many errors such as failure to enroll (FTE), false accept rate (FAR) and false reject rate (FRR) represent examples of ways in which performance of a biometric system can be degraded. Performance is not a static value, when biometric systems are concerned, as it depends in numerous factors such as the quality of the captured signals/images, the composition of the target user population (gender, race, age, profession, etc.), the number of subjects enrolled (size of the database), the temporal gap between enrollment and identification (as the measured traits might, even though they should not, be time variable), the environmental conditions under which the identification process is carried (temperature, humidity, illumination, etc.), the operating mode of the biometric system in a given situation (verification or recognition) and the robustness of the employed algorithms (how well they behave under distinct conditions than the ones they were created and tested under). Performance measurements will be addressed in more detail in subsequent sections.

2. *Cost:* costs associated with the development and implementation of a biometric system arise mainly from the direct components such as hardware components (sensor, processor, memory) and software blocks (graphical user interface and matcher) and the indirect components, which include system installation, training/maintenance and user acceptance. The decision regarding investment on a biometric system will be heavily weighted on how the

chosen components will affect the performance of the system and how these effects will condition the return cash-flow associated with its implementation.

3. *Interoperability:* with a wide range of applications to cover a biometric system should be capable of functioning in an interoperable way, without the assumption that the same sensor, algorithms or operating conditions will be available during the entire length of its lifetime. The interoperability of a biometric system is based in the idea that a system should be able to perform identification using sensors from different brands and on a broad spectrum of hardware and software platforms. Achieving this ideal state would have a deep effect in both costs and performance, as no alternative software development would be needed to adapt the system to new conditions.

4. *Acceptability:* Some considerations must be taken into account to try and improve the social acceptability of a biometric system - Hygiene and health conditions when several individuals need to contact the same sensor (main reason why contactless fingerprint sensors started to emerge); Acquisitiveness conditions, as not all biometric traits are so easily captured as others; Ergonomic, accessibility and user friendliness factors, such as physical and logical access control, as no one should be unable to use the biometric system because of physical or mental disorders.

5. *Circumvention/Security:* biometric systems should offer a high degree of protection against intrinsic failures of the system in face of adversarial attacks (circumvention). This is especially important when the security of the biometric template database is concerned, and only personnel with the highest level of security access should be able to directly contact it.

2.3.4 Evaluation methods

As it was mentioned in the previous section, performance is an indispensible requirement for the development of a biometric system. The main question regarding performance is how to quantitatively present this information, as a wide variety of factors influence it. Considering a known set of conditions, under which a recognition process is being carried by a biometric system, there are two simple classes of errors: a false match, in which the matcher declares a match between two different biometric signatures, and a false non-match, where the system is unable to identify two equal biometric signatures as belonging to the same individual (Jain and A., 2010). Two quantitative measurements can be defined to assess the rate of false matches and false non-matches: the false match (or false accept) rate (FMR/FAR) and false non-match (or false reject) rate (FNR/FRR), respectively. Mathematically, these values can be calculated by Equations 2.1 and 2.2 respectively:

$$FAR = \frac{FA}{FA + TI} \tag{2.1}$$

$$FRR = \frac{FI}{FI + TA} \tag{2.2}$$

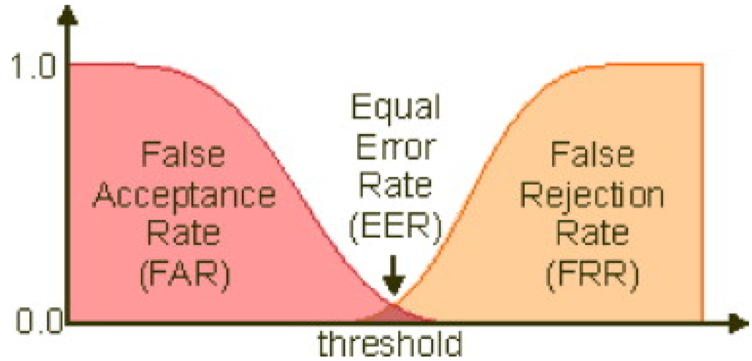

Figure 2.6: Graphical representation of the evolution of FAR and FRR values for distinct similarity threshold values (Nanni and Lumini, 2009).

where *FA* and *TA* are the number of falsely accepted and correctly accepted users respectively and FI and TI are the falsely considered and correctly detected impostors respectively. The way these two types of errors are balanced depends on a single parameter: the similarity threshold (T). This is the measured similarity value above which two biometric signatures are considered to belong to the same individual and below which they are considered to belong to distinct individuals.

For low T values comparisons with low similarity values will result in a match. This way many matches will be made between impostors and authorized individuals because little similarity will be enough to trick the system. On the other hand with low T values few authorized individuals will be rejected by the system, because even if they present small similarity values they will still be considered matches.

The same rationale can be used to understand what happens with high T values: in this case matches will be only made for high similarity values. This results in fewer impostors being identified as authorized individuals, unless they somehow present high similarity value with some identified subject, and higher probability of someone with access not being identified as such even if the similarity value is reasonably high. These trends of FRR and *FAR* variation can be plotted against variable values of T (Figure 2.6).

It can be observed that the two resulting curves intersect in a specific point, in other words, a point where the FRR and *FAR* values are equal. The FRR/FAR error value observed in this point is called the equal error rate (EER), a very common performance measure in biometric systems. Another typical performance measurement representation is the area under the receiver operating characteristic (*ROC*) curve. The *ROC* curve is obtained by plotting a *FAR* vs. FRR curve, as exemplified in Figure 2.7 (Jain et al., 2000; Proença, 2007; Jain et al., 2006).

Even though the *EER* finds the optimal T value to optimize both FRR and *FAR* at the same time, some applications of biometric systems seek to minimize only one of these parameters, with little or no interest in the other. Forensic applications, for example, cannot accept the mistake that a criminal is not identified as himself. Therefore forensic biometric systems generally work at fairly low *FRR*/fairly high *FAR*. High security systems on the other hand are more interested in not allowing unauthorized personnel to access restricted information. These biometric systems

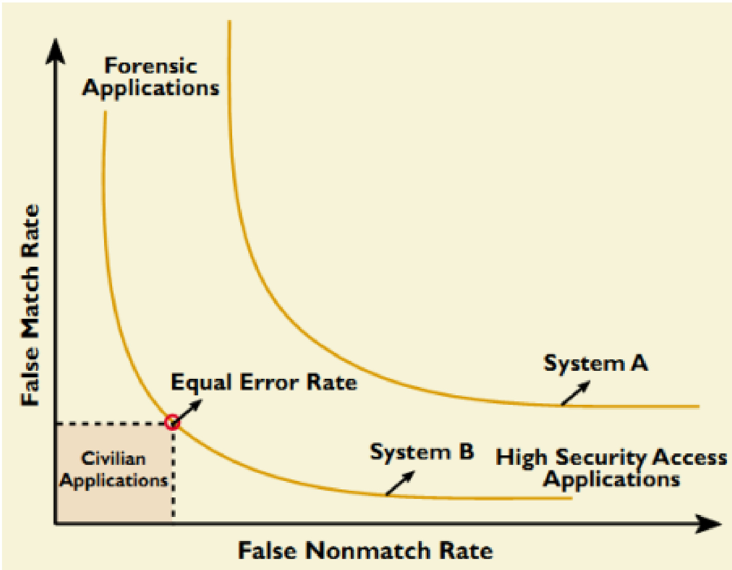

Figure 2.7: Examples of receiver operating characteristic (ROC) curves for two biometric systems (Jain et al., 2000).

work, therefore, at low *FAR*/ high *FRR* values. Thus, the intended application is an important factor that affects both development and performance evaluation of biometric systems (Jain et al., 2000).

The *FAR* and *FRR* evaluation measurements are the most common indicators of recognition accuracy when the biometric system is meant for verification mode. When working on recognition mode the ratio between number of wrong recognition attempts and the total number of recognition attempts, also known as the false identification rate (FIR) is the most commonly used and meaningful variable (Proença, 2007).

Apart from false match, false non-match or false identification, some other big classes of errors can be assessed to characterize the accuracy of a biometric system. The failure to capture/acquire (FTC/FTA) rate and the failure to enroll (FTE) rate are two of the most commonly used. The FTC rate is only applicable when the biometric system presents automatic capture functionality and denotes the percentage of times the device fails to acquire a sample when the biometric trait is presented to it, either because of the sensor not being able to locate the biometric trait or because the acquired data is not of sufficient quality. The FTE rate, on the other hand, relates to the users who are not able to perform the enrollment process. These errors happen, generally, when the system rejects poor quality inputs during enrollment. A direct consequence from this selection during the enrollment process is that the quality of the templates comprising the database is generally high. A high quality template database causes the system accuracy to improve, as low quality template data is prone to present low similarity values even when better quality signatures from the same individual are presented to the biometric system (Jain et al., 2006).

2.4 Biometric traits: a comparative approach

As it was seen in previous sections all biometric traits that respect the four requirements – universality, uniqueness, collectability, permanence – can be considered in the development of a biometric identification system. In this section some of the most commonly used biometric traits (Figure 2.8) are presented in detail under the considerations set by these four requirements. In the end of this section the pros and cons of every trait are summarized in Table 2.1, in an update of the table presented in (Jain et al., 2000) with additional data from (Proença, 2007).

2.4.1 DNA

The deoxyribonucleic acid (DNA) of every human is a unique sequence of nucleotides of four types – amine (A), thymine (T), cytosine (C) and guanine (G) – distributed among 23 pairs of chromosomes (one inherited from the mother and one from the father) and coding the information for every biological process of the organism (Seeley et al., 2007). Approximately 99.9% of the DNA content is conserved between every human being, but the remaining 0.10% differs and is responsible for the phenotypic differences between individuals (such as eye color, hair color, skin pigmentation, etc.). The only exception to the uniqueness of DNA is the one related with homozygotic twins who have exactly the same genetic code, rendering DNA biometric systems useless in such cases (which might cause serious repercussions ifsecurity applications are the objective) (Proença, 2007; Jain and A., 2010). DNA extraction presents some serious drawbacks: it is not an automated process, it carries high associated costs, it is a very time consuming process, and the possibility of DNA contamination during the handling of samples is significant (Jain and A., 2010).

2.4.2 Ear

Ear recognition can be achieved by the analysis of three types of data: photos of ears, earmarks against flat surfaces and thermograms, three simple procedures that can, however, be obstructed by some less ideal acquisition conditions: hair or ear muffles can cover, partial or totally, the area of the ear or the ear can be slightly rotated, disabling the system capacity to identify the tested subject (Proença, 2007; Arbab-Zavar and Nixon, 2011). Nevertheless some main advantages characterize ear recognition: the dimensions of the images to process are relatively small (decreasing processing time), the structure is relatively permanent with increasing age and practically every human being has ears. The question of ear uniqueness was studied by Alfred Ianarelli in 1989 (Iannarelli, 1989), who concluded, after analyzing 10000 ear images, that enough dissimilarity between ear patterns for their use in biometric systems. Even in twins, who generally share many anatomical traits, ear patterns seemed to provide a good tool for identification, especially in the concha and lobe areas (Proença, 2007; Geng, 2010).

2.4.3 Face

Face recognition is probably the oldest and most intuitive recognition process for mankind. Facial recognition in biometric systems generally takes advantage of spatial relationship among anatomical traits such as eyes, nose, lips or chin or from general characteristics based on edges, lines and curves to distinguish between individuals. Problems associated with these methods arise from unconstrained data acquisition which yields different capturing angles, illumination conditions, facial expressions, makeup usage and partial occlusion, or from the uniqueness problems connected to twin brothers or modified faces through plastic surgery. The main advantages of this trait for biometric applications are the high social acceptability of facial recognition, the non-intrusive nature of the process and the existence of widely used databases, such as the FERET database, the standard database for facial recognition algorithm efficacy comparison (Proença, 2007; Jain and A., 2010).

2.4.4 Facial thermogram

Capturing face images using an infra-red camera produces a unique facial signature, as a consequence of a unique vascular structure observed in each face, as heat passes through the facial tissue and is emitted from the skin. These signatures are called facial thermograms. As the heat pattern is emitted from the face surface, without any source of external radiation, these systems can capture good quality images despite the external conditions of illumination. It is a non-invasive method with possible application in covert recognition and it is less vulnerable to disguises such as plastic surgery. Some disadvantages may arise from acquisition near external sources of heat, emotional state of the tested subject and off-angle faces, besides the inevitable problem of permanence (as face changes with time, so does the vasculature pattern (Buddharaju et al., 2007). However, facial thermogram represents an improved biometric trait over its counterpart (facial recognition): it works in a considerably less restricted set of conditions and presents a considerably higher difficulty of forging (Proença, 2007; Seal et al., 2011).

2.4.5 Hand geometry

Hand shape, alongside finger length and width are some of the most commonly used human hand measurements in biometric systems. The main advantages of hand geometry are the relatively high independence from the acquisition environment conditions (factors such as dry skin play no important role in defining the geometry of the hand), the ease of use and the low costs associated with the development of such systems. All these advantages are counterbalanced by its main disadvantages: low discriminating capacity, variability over an individual's lifespan, restrictions regarding jewelry use or dexterity limitations, etc. The development of unconstrained methodologies for hand geometry application in biometric systems have focused on the development of deformable models for hand segmentation (Proença, 2007) and the creation of contact-free scenarios, where no platform and pegs for hand positioning are necessary to acquire hand geometry information (thus demanding almost no collaboration from the user). Contact-free scenarios allow the avoidance of hand distortion and lower the hygienic concerns, often associated with social acceptability (de Santos Sierra et al., 2011).

2.4.6 Palmprint

Palmprint patterns, composed of principal lines, wrinkles and textures, have some interesting features for application in biometric identification systems: the principal lines structures are stable across an individual's lifetime and the social acceptability regarding palmprint scanning does not constitute a problem. Although palmprint systems are not as widespread in civilian applications, such as access control (Proença, 2007; Jain and A., 2010), as fingerprint systems, research is being conducted with the objective of increasing discriminating capacity of such systems, and palmprints represent, thus, a promising approach for medium-security access-control (Proença, 2007). One of the main issues about palmprint recognition is the relatively large size of the required sensors, when compared to the ones used in fingerprint recognition (Jain and A., 2010).

2.4.7 Hand veins

The vein pattern that characterizes each individual's hand can be easily acquired using near-infrared radiation, which illuminates the palm and captures the light that diffuses across the hand (Proença, 2007; Jain and A., 2010). Deoxidized hemoglobin, one of the main constituents of the organic phase of venous blood (Seeley et al., 2007), has a peak of absorption for wavelengths in the infrared range, thereby reducing the reflection rate of NIR radiation near veins, causing them to appear black in the resulting image. Observed vein patterns are generally stable amongst adults but begin to shrink as a result of reduction in bone and muscle strength at older ages, and can be severely influenced by some pathological conditions affecting blood vessels like diabetes, atherosclerosis or tumors (Proença, 2007). Some concerns regarding biometric systems based in vascular patterns arise due to the high expected costs associated with their development and the lack of large scale studies on vein individuality and stability. User acceptability is one of the main advantages as these systems are contactless, thus overcoming the hygiene concerns of some more common systems (Jain and A., 2010).

2.4.8 Fingerprints

Fingerprints are universal to all people, unique and stable throughout a person's lifetime, and have, thus, been the most commonly used trait in the development and implementation of biometric system in civilian activities (Ailisto et al., 2006). Their unique characteristics arise from the pattern of ridges and valleys on the surface of a fingertip, which are defined, by partially random morphogenesis processes, in the first seven months of fetal development, creating a unique pattern even in homozygotic twins. In the past these patterns were extracted by inked impressions of fingertips on paper, but today, compact sensors are already available to readily acquire digital images of fingertips. Image analysis is generally performed over specific critical points, commonly designated minutiae points, which are related to either ridge bifurcation or ridge ending motifs Proença (2007). Some disadvantages concerning fingertip biometrics are related with the considerable computational requirements that these systems present, especially when operating in identification mode, and also with the considerable ease of mutability in the patterns, as a result of occupational (manual workers tend to develop large number of cuts, bruises, etc.), environmental (burns in fingertips will mask the fingerprint pattern) or aging (wrinkled surfaces are harder to recognize) factors (Jain et al., 2004).

2.4.9 Iris

According to the biometric literature, the iris's structural texture is significantly variable across the population. Even the irises of monozygotic twins exhibit structural differences, suggesting that random events play a significant role in the morphogenesis process of the trabecular meshwork (see Section 3.1) which defines the observed iris patterns under visible light. Such a high degree of uniqueness is however constrained by the acquisition condition: the quality of the iris image must be strictly monitored to ensure reasonable textural detail (Ross, 2010). To improve the quality of these images, near-infrared (NIR) light is typically chosen for illumination, as it is detectable by most cameras but not by the tested subject (Proença, 2007). It is almost impossible to surgically alter iris texture information and algorithms for artificial/fake iris (such as printed pictures) detection are already developed (Lee et al., 2006) and even blind people can use iris recognition systems (Mastali and Agbinya, 2010). Early problems related with user collaboration and high associated costs are already being overcome with the development of user-friendly/cost-effective versions (Proença, 2007).

2.4.10 Signature

Signature is a behavioral biometric modality that is used daily in many applications like business transactions. Two major strategies for signature recognition can be distinguished: image-based and dynamics analysis. The first is the most common method and is based on the visual appearance of the signature. The latter analyzes speed, direction and pressure of writing (Proença, 2007). Attempts to develop accurate automatic signature-based biometric systems have been far from successful. The large intra-class variations in a person's signature over time are one of the main causes. Attempts have been made to improve performance by capturing dynamic signatures on a pressure-sensitive pen-pad. Dynamic signatures help in acquiring the shape, speed, acceleration, pen pressure, order and speed of strokes, during the actual act of signing. This new information (speed, acceleration, pressure, stroke order, etc.) seems to improve the verification performance as well as circumvent signature forgeries (Jain and A., 2010). One of the main advantages that separates signature from more traditional biometric traits is the fact that it can be changed, like a password, in a way that iris or fingerprint cannot (Proença, 2007).

2.4.11 Retina

Retinal scans detect the blood vessel patterns in the posterior part of the eye which are stable along an individual's lifetime (except in the case of vessel related diseases (Jain et al., 2004)) and unique between individuals in a population (Proença, 2007) but whose acquisition involves cooperation, contact with the eye-piece, and a conscious effort on the part of the user. All these factors contributeto the low acceptability and user unfriendliness that characterize these systems (Jain et al., 2004). However the big advantage of retinal systems is the fact that this anatomical trait is protected by the eye and is therefore very difficult to access and modify or replicate. Its main applications are therefore high-security related, like access to prisons (Jain et al., 2004; Proença, 2007).

2.4.12 Keystroke

It is believed that everyone types on a keyboard in a unique way (Proença, 2007). The analysis of the dynamics of typing, such as rhythm and pressure analysis, might serve as an indication of a subject's identity (Proença, 2007; Jain et al., 2004). This behavioral trait might encounter some adversities, such as large typing pattern variations for the same individual, and privacy concerns related to some activities that such a technology would allow (analyzing someone's typing pattern would allow a tool to quantify his/hers work effectiveness). The main advantage of keystroke is that it allows continuous scanning and monitoring, reducing the risk of counterfeit, and is generally well accepted, as people already interact with keyboards in more traditional security systems (i.e. passwords) (Proença, 2007).

2.4.13 Gait

Gait is the characteristic periodic set of leg movements each individual presents while walking. Information regarding shape (relative position of several anatomic markers, such as joints) and dynamics (cycle time, rhythm variations, etc.) can be used to distinguish between individuals, even though it is only used for verification in low-security applications. This behavioral trait is not time invariant: fluctuations in body weight, possibility of brain or joint injuries or surface irregularities, among others, are certain to influence the gait pattern. The permanence of gait is questionable, as an injury might cause an individual to inadvertly change its common gait pattern, thus risking an erroneous output from the recognition system. As many articulations are likely to be analyzed to overcome all these difficulties, a high computational cost is generally associated to such applications. The great advantage of gait analysis is connected to the ease of collectability for such images, as any common camera will be enough for the desired analysis (Jain et al., 2004; Proença, 2007).

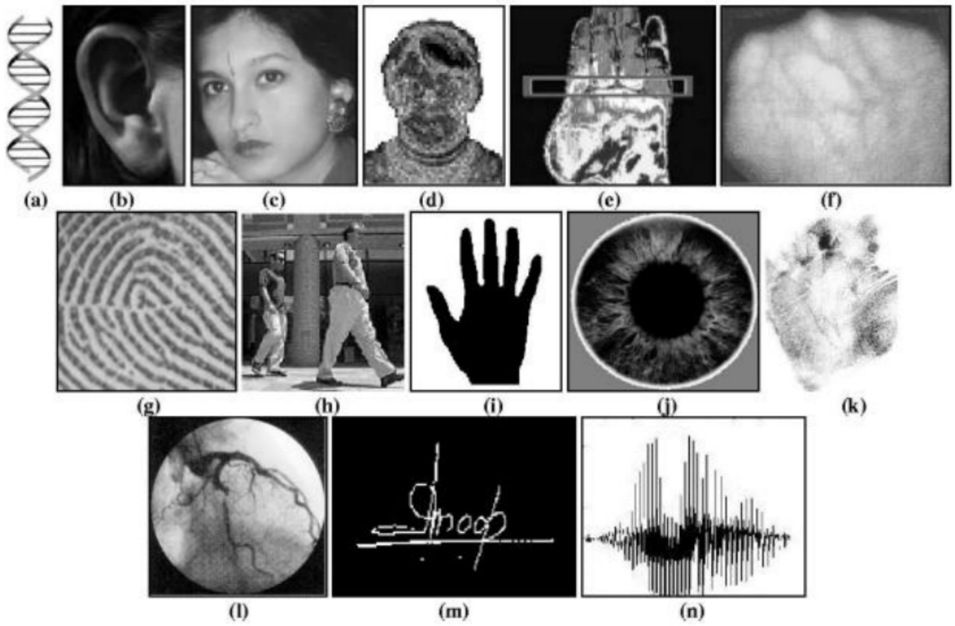

Figure 2.8: Several biometric traits (extracted from (Jain et al., 2004)): (a) DNA; (b) Ear; (c) Face; (d) Facial thermogram; (e) Hand thermogram; (f) Hand veins; (g) Fingerprint; (h) Gait; (i) Hand Geometry; (j) Iris; (k) Palmprint; (l) Retina; (m) Signature; (n) Voice.

2.4.14 Voice

Voice is a particular case of a biometric trait, as it is acoustic based, instead of image-based as the majority of the most commonly used biometric traits (Proença, 2007). Even though the anatomical features that define each individual's voice (vocal tract, mouth, nasal cavities, etc.) are relatively stable during adult lifetime, behavioral changes affect speech features, as a result of aging, medical conditions and social environment. Voice recognition systems are generally divided into text-dependent, where recognition is performed using a pre-read phrase as template, and text-independent, which is harder to circumvent but lacks the accuracy of its text-based counterpart (Jain et al., 2004). Acquisition conditions also play a major role in the success of speech recognition systems: simple background noise might compromise all the acquired data. Currently existing applications focus on the telecommunication industry (Jain et al., 2004; Proença, 2007).

2.4.15 Comparative analysis

The characterization of the multiple traits presented in previous sections is summarized in Table 2.1. When choosing the biometric trait to serve as the basis for a recognition system one must ask which of the 4 criteria (universality, uniqueness, collectability, permanence) is indispensable and which other criteria can be more or less overcome by the developed algorithms. Analyzing Table 2.1 it can be noted that ear, hand geometry, iris, palmprint and hands veins are the only traits with no criteria classified as 'low'. However, with this simple discrimination, facial thermogram, which presents a 'high' universality, uniqueness and collectability, for example, is easily ruled out.

The choice must, thus, be made, by considering what is more important for each specific application. In the present dissertation the choice of working with iris rose from the fact that this trait excels in universality, uniqueness and permanence, even though the collectability of good quality images is conditioned by the use of complex acquistion devices. As the proposed worked aimed to iris recognition under unconstrained settings, the collectability problems with iris became less problematic, as it is proposed that the algorithms are able to work under less ideal acquisition settings. Giving less importance to the collectability as a criteria for the choice of a biometric trait, the iris becomes the primary candidate from the traits described in previous sections.

Table 2.1: Comparative data analysis of the afforementioned biometric traits. Data adapted from (Proença, 2007) and (Jain et al., 2000)

	Requirements			
Trait	**Universality**	**Uniqueness**	**Collectability**	**Permanence**
DNA	High	High	Low	High
Ear	Medium	Medium	Medium	High
Face	High	Low	High	Medium
Facial Thermogram	High	High	High	Low
Hand Geometry	Medium	Medium	High	Medium
Iris	High	High	Medium	High
Palmprint	Medium	High	Medium	High
Signature	Medium	Low	High	Low
Hand Veins	Medium	High	High	Medium
Keystroke	Low	Low	Medium	Low
Retina	High	High	Low	Medium
Gait	Low	Low	High	Low
Voice	Medium	Low	Medium	Low

Chapter 3

Iris Recognition State-of-the-art

3.1 Eye and Iris anatomy

The human eye (Figure 3.1) is composed by three layers or tunics: the external layer or fibrous tunic, constituted by the sclera, and, in its anterior part, by the cornea; the middle layer or uvea/vascular tunic, composed by the cilliar body and the iris; and the internal layer or the nervous tunic, where the retina is found (Seeley et al., 2007). In a typical non-invasive image of the eye (Figure 3.2) three anatomical features are visible: the sclera, the iris and the pupil.

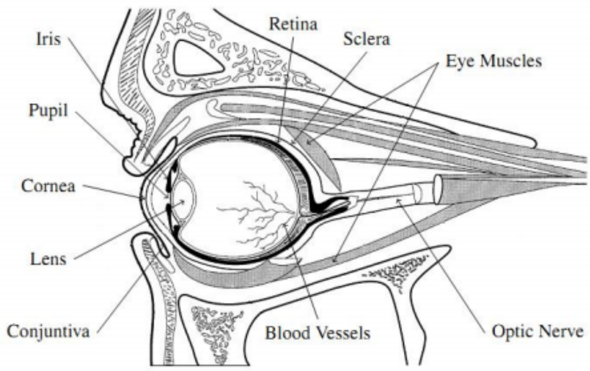

Figure 3.1: Eye anatomy (Proença, 2007).

The sclera is the external, firm, opaque and white posterior layer of the eye. It consists in conjunctive tissue, made of collagen and elastin fibers, and its main roles are the maintenance of the three-dimensional structure of the eye and the connection with the insertion points of the muscles responsible for eye movement (Seeley et al., 2007). The iris is the colored part of the eye and its denomination comes from the fact that its color difers between individuals (Gray, 2010). Brown eyes possess a brown melanin pigment, absent in blue eyes, where the color derives from a light diffraction process similar to the one observed in the atmosphere and that confers the sky its color. It's a contractile structure mainly composed of smooth muscle, surrounding an aperture, known as the pupil. Light penetrates the eye through the pupil and the iris regulates the quantitiy of light by adjusting the size of the pupil (Seeley et al., 2007). The iris begins to form during the third month of gestation and the structure is complete by the eighth month, although pigmentation continues into the first year after birth. The visible features of the iris arise from a complex trabecular meshwork of connective tissues whose complex and unique patterns are seen under visible light illumination of the iris (Proença, 2007).

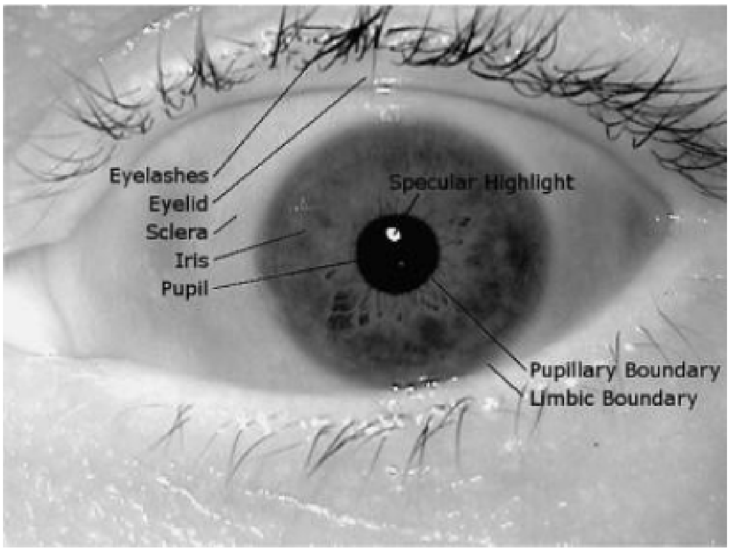

Figure 3.2: Typical eye photograph (Bowyer et al., 2008).

3.2 Pioneer works on iris recognition

3.2.1 Daugman's method

In 1987 American ophthalmologists Flom and Sair patented a concept (Flom and Safir, 1986), developed in 1949 by James Doggart (Doggart, 1949), concerning the possibility of using the complex patterns of the iris in a similar way as fingerprints, to develop accurate recognition systems. The first algorithm to take advantage of this concept was published in 1993 by Professor John Daugman (Daugman, 1993), of Harvard University, who would later patent it in 1994 (Daugman, 1994).

Daugman's earlier work (Daugman, 1993) established the main principles for almost every iris based biometric system. The main steps of the algorithm are schematized in Figure 3.3.

The iris localization and segmentation assumed the pupillary (Iris-Pupil) and limbic (Sclera-Iris) boundaries of the eye as circles, described by three parameters: the radius r, and the coordinates of the center, x_0 and y_0. He proposed an integro-differential operator (Equation 3.1) that searched the parameter space for the values that maximized:

$$G_\sigma * \frac{\delta}{\delta r} \cdot \oint_{r_0,x_0,y_0} \frac{I(x,y)}{2\pi \cdot r} \cdot ds \tag{3.1}$$

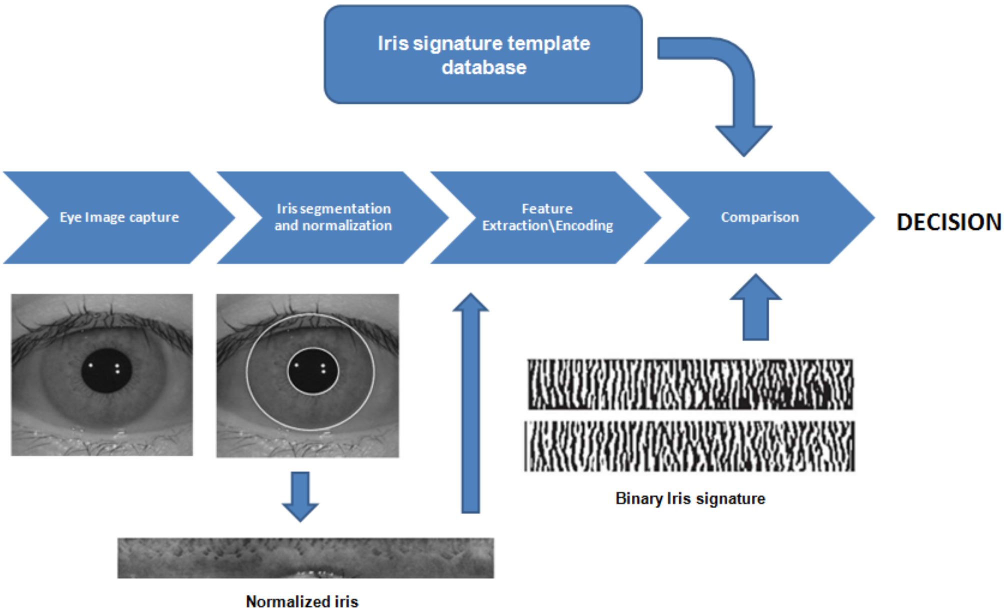

Figure 3.3: Schematization of Daugman's iris recognition method. The global steps presented can be extrapolated to almost every iris recognition algorithm. Image adapted from (Chang et al., 2009) and (Ross, 2010).

In the formula of the integro-differential operator I symbolizes the original iris image, G_s is a low-pass Gaussian filter, used for smoothing, with s standard deviation and is the convolution operator. The Daugman operator would therefore compute, for each possible combination of x_0, y_0 and r the total "energy" of a closed contour (line integral) centered on (x_0, y_0) with radius r, choosing the maximum variation in this parameter along the possible radius values, as the optimal r for the chosen (x_0, y_0) center. The (x_0, y_0, r) triplet candidates yielding maximum results for the integro-differential operator would be assigned to the limbic and pupillary boundaries of the eye. From this information the iris could be easily isolated, in a process denominated iris ***segmentation***.

The following step consisted in coding the information contained in the segmented iris region in a way that made it possible to compare between individuals. Some problems appear during this process when different iris' sizes are observed or when the dilation or contraction of the iris (as a result of non-uniform illumination) is variable (Bowyer et al., 2008). Daugman suggested a normalization step, known as the rubber sheet model (Figure 3.4), to overcome these limitations: every location on the iris image was defined by two coordinates, relative to the previously detected (x_0, y_0) iris center – an angle θ between 0 and 360 degrees, and a radial coordinate ρ ranging between 0 and 1, normalized to the radius of the iris. For each ρ, n discrete points are chosen along the radial line that goes from $\rho = 0$ to $\rho = 1$. Using this coding technique, regardless of the size of the iris or its contraction level, a $n \times \theta$ rectangular image containing all the iris information is obtained (Proença, 2007; Ross, 2010; Daugman, 1993; Bowyer et al., 2008).

Once the normalized image is computed, Daugman suggests the use of 2D Gabor filters (Gabor, 1946) for texture analysis and feature extraction. To optimize computing times and lower

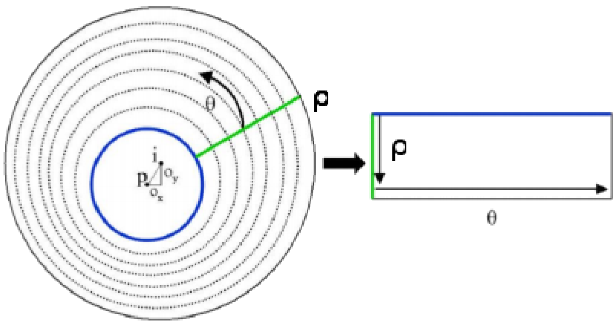

Figure 3.4: Daugman rubber sheet model. Adapted from (Velho, 2009).

calculation complexity, the resulting phase response to each Gabor filter was summarized in 2 bits: each pixel is assigned 1 to the first bit if the real part of the phase response is positive and 1 to the second bit if the imaginary part is real (Figure 3.5). Thus, for every iris image a simple binary code was obtained, and the matching process against iris templates was performed by simple bitwise operations.

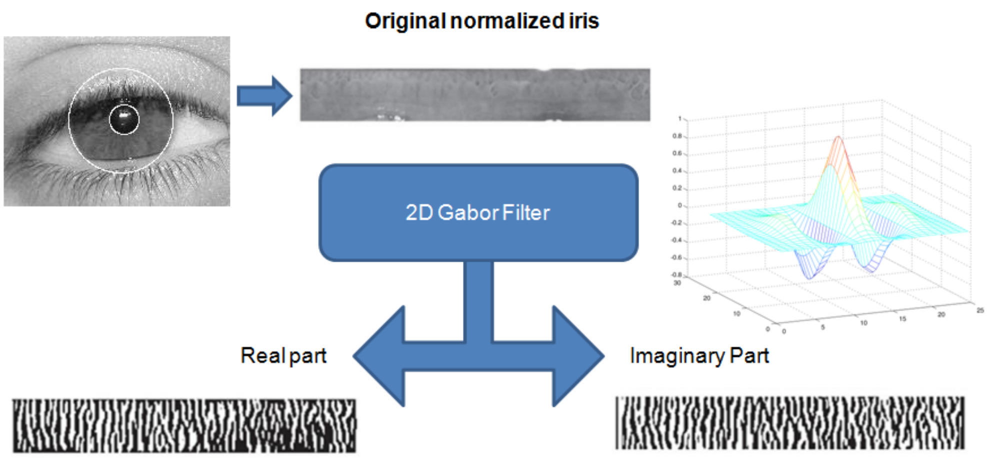

Figure 3.5: Schematization of the encoding process of the normalized iris image using bidimensional Gabor filter. Image adapted from (Ross, 2010).

The dissimilarity measurement used by Daugman was the normalized Hamming distance (Equation 3.2), which measures the fraction of bits where the two binary codes from iris signature and iris template disagree (Proença, 2007; Daugman, 1993; Bowyer et al., 2008). Such a simple way to quantitatively measure dissimilarity was only possible due to the binarization step of the Gabor filter response.

$$HD(A,B) = \frac{1}{N} \cdot \sum a_i \otimes b_{i_{i=1}}^{\ n} \tag{3.2}$$

This pioneer work set the basis of the typical iris recognition system architecture: segmentation, normalization, feature extraction and matching are the four main components of every system. Almost every commercially available iris recognition system nowadays is based on Daugman's patented system (Daugman, 1994). The results for this method, under optimal conditions are presented in Figure 3.6 with an equal error rate of 1 in 131.000 (Daugman, 1994), for a dataset of 2064 iris signatures.

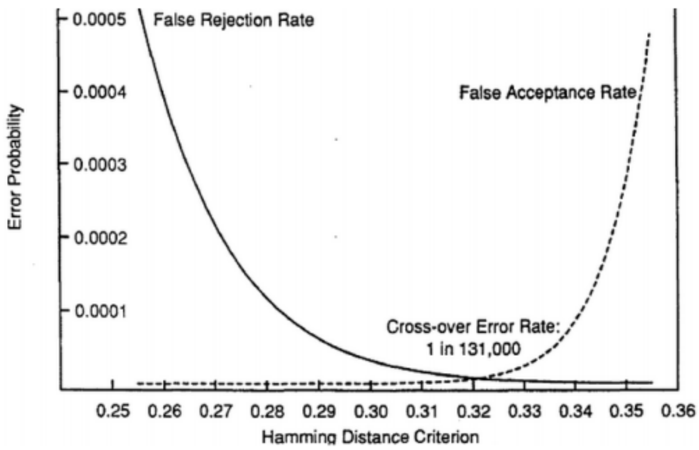

Figure 3.6: FAR vs FRR results in Daugman's patented method (Daugman, 1994).

3.2.2 Wildes' method

Alongside Daugman's method as a classical approach to iris recognition, a very distinct approach was taken by Richard Wildes in 1997 (Wildes, 1997). The acquisition module used by Wildes captured images that comprised not only the iris but also surrounding structures of the eye. The segmentation is accomplished by first converting the iris image into a binary edge map. This is accomplished by convolving a Gaussian-derivative filter (which enhances edges/high frequency areas), weighting the horizontal and vertical components of the gradient operator for preferential directional enhancement, with the original image, and then applying a simple threshold for binarization. The limbic contour is then assessed by a maximization process similar to the Daugman integro-differential operator. The parameters for such maximization are here represented by r, x_c and y_c, and are used by a different scoring method, namely the *Circular Hough Transform*, *CHT*:

$$H(x_c, y_c, r) = \sum_{j=1}^{n} h(x_j, y_j, x_c, y_c, r) \tag{3.3}$$

$$where, \tag{3.4}$$

$$h(x_j, y_j, x_c, y_c, r) = \begin{cases} 1, if g(x_j, y_j, x_c, y_c, r) = 0 \\ 0, otherwise \end{cases} \tag{3.5}$$

$$and, \tag{3.6}$$

$$g(x_j, y_j, x_c, y_c, r) = (x_j - x_c)^2 + (y_j - y_c)^2 - r^2 \tag{3.7}$$

The *CHT* checks every pixel resulting from the edge map binarization as a possible (x_c, y_c) combination, that is, as a possible center for the iris. It then counts the number of pixels (x_j, y_j) with value 1 that can be found in a circular region with radius r centered on the tested (x_c, y_c) candidate. The algorithm will return an accumulator array, H, with a scoring value for each (x_c, y_c, r) triplet. The global maximum of the accumulator array is identified as the most probable candidate for limbic boundary.

The normalization step in this method consists in an image registration process, where a mapping function is applied to the original image to compensate translational and scaling differences between acquired images and database templates. The translation and scaling functions are chosen so that corresponding pixel's intensity in the signature image, I a , and the tested database image, Id , is as close as possible. Feature extraction is accomplished by a multi-spectral analysis of the segmented iris using Laplacian-of-Gaussian (LoG) filters with distinct sizes and s values. The matching is accomplished by normalized correlation between Id and normalized Ia, the result of which will express a similarity value between the two matched images. Results from Wildes' works reveal a higher EER value (1,76% (Ma et al., 2004)) when compared to the one obtained with Daugman's patented system. However there are some functional advantages to Wildes' method. Table 3.1 summarizes the pros and cons of Wildes' method when compared to Daugman's (adapted from (Bowyer et al., 2008)).

Table 3.1: Pros and cons of Wildes' method when compared to Daugman's method.

Wildes' method	
Pros	***Cons***
Less intrusive light source	More complex acquisition system
Removal of specular reflections	Smaller sensitivity to some details (as a result of binary edge map abstraction)
Segmentation is more stable to noise perturbations	Less compact representation of iris features
Capable of finer distinctions (Multiple LoG filter responses are not binnarized)	Higher computational cost
Better adaptability to real world situations (Image registration)	

3.3 Recent works on iris recognition

The original approach to the segmentation task made by Daugman (1993) consisted in the use of an integro-differential operator. In a different approach, Wildes (1997) suggested a method involving edge detection followed by circular Hough transform (CHT). For years, many works in the iris biometrics area focused on Daugman's and Wilde's algorithms, presenting variations at many levels.

Tan et al. (2010) first extracted a rough position of the iris by performing a clustering-based scheme and then localised the pupillary and limbic boundaries using a new constructed integro-differential operator. In the work of He et al. (He et al., 2009), an Adaboost-cascade iris detector is built to extract a rough position of the iris centre and then the centre and radius of the circular iris are localized by employing an elastic model named *pulling and pushing*. The segmentation of the pupil and iris by fitting a rotated ellipse after a sequence of procedures for compensating the detected noises was proposed by Zuo and Natalia (Zuo and Schmid, 2010). In a different approach, Roy et al. (Roy et al., 2010) consider the iris as a non-circular structure and use an elliptic fitting model to fit both the limbic and pupillary contours. Then they perfect it by a geometric active contour procedure based on Chan-Vese's energy minimization process. Krichen et al. presented a work (Krichen et al., 2009) based on Gabor filter phase response for iris localization. The segmentation step was an altered version of the CHT-based Masek algorithm (Masek, 2003). In their work, Ma et al. (Ma et al., 2004) created a system that mixed both the CHT segmentation approach and the rubber sheet model normalization, introducing some concepts like pre-processing of iris images for specular reflection removal. In the work of Abhyankar et al. (Abhyankar and Schuckers, 2009) segmentation starts with the transformation of the iris image into the wavelet domain and enhancement of image contours by a process of in-band denoising, which works by thresholding and filtering low energy components of both high and low frequency components. The Canny edge detector is then applied to the enhanced image and CHT is used for the detection of both iris boundaries. The approach taken by Chen et al. (Chen et al., 2010) starts by detecting the sclera region of the eye, thresholding and filtering the image to detect a rectangular region for iris localization. An edge map of the region of interest is then obtained with a horizontal Sobel operator, and a dynamic programming variation of the CHT algorithm was implemented to detect the limbic boundary. This method corrects the non-circularities of the off-angle iris and combines the intersection of circles obtained by the two CHT algorithms and a linear Hough transform to perform eyelid detection.

Since iris boundaries are often not circular or elliptical, curve fitting techniques can be valuable to approximate real iris contours (Proença et al., 2010). To further improve the segmentation performance, recent methods attempted to use active contour models to accurately localise irregular iris boundaries (Daugman, 2007; Vatsa et al., 2008; Houhou et al., 2008; Shah and Ross, 2009). A illustrative example for limbic and pupillary contour detection was presented by Lu and Lu (Lu and Lu, 2008): first they use a deformable model (snake), which requires the manual definition of a starting contour which is then optimized through an iterative energy minimization process based on image gradient and snake bending (Kass et al., 1988), to detect the pupillary contour; finally, they apply the integro-differential operator suggested by Daugman to detect the limbic boundary.

Some works use texture analysis to perform segmentation. Nabti and Bouridane's work (Nabti and Bouridane, 2008) is based in a multiscale approach, using Gabor filters and wavelet transform coefficients, to improve edge detection process that determines the success of iris segmentation. A work based on dyadic wavelet transform zero-crossing as iris signature was published by Roche et al. (Sanchez-Avila et al., 2002) where images were pre-processed by histogram stretching (improving contrast between pupil, iris and sclera) before the limbic boundary detection. After this contour is detected, the same algorithm is used inside its area to detect the pupillary boundary. The iris localization method by Guo and Jones (Guo and Jones, 2008) is based on intensity gradient and texture difference, using the standard integro-differential operator.

In the work of Tan et al. (Tan et al., 2010), segmentation was divided into four main blocks. The first step consisted in a region growing based algorithm to distinguish between iris candidates and the remaining image. The regions resulting from this iterative process are then analysed for specific iris characteristics, such as roundness and relative position to other regions (for example, eyebrows could be distinguished from the iris as they are a dark region, horizontal, placed above the iris). The second step consists in iteratively finding the shortest path that maximizes the Daugman integro-differential operator so that the limbic and pupillary boundaries can be detected. The next steps deal with eyelid/eyelash detection and removal.

A gradient vector field based method appears in the work of Chen et al. (Chen et al., 2011). In this work the iris template gradient allows the detection of iris borders, but was not tested for detecting the iris center, probably because the images in the selected database (CASIA, 2004) have a very well defined pupil (as the value of pixels in that area is set to zero).

When analysing much cited methods in the literature is possible to detect some of their main drawbacks. In almost all of these methods, inner and outer boundaries, eyelashes and eyelid are detected in different steps, causing a considerable increase in processing time of the system. Usually, the inner and outer boundaries are detected by circle fitting techniques. This is a source of error, since the iris boundaries are not exactly circles and, in noisy situations, the outer boundary of iris does not have sharp edges. (Barzegar and Moin, 2008)

In some of the aforementioned algorithms, there are a lot of implicit or explicit assumptions about the acquisition process, which are no longer valid in unconstrained acquisition scenarios. Therefore, some of the promising results reported in the literature must be taken with caution and reassessed under these new, more challenging, conditions.

3.4 The path forward

A lot of conditions are involved in the acquisition of the iris images that were used in the development of the aforementioned algorithms:

- Image acquisition uses NIR illumination so that illumination can be controlled without human perception. Near-infrared illumination also helps reveal the detailed structure of heavily pigmented irises. Melanin pigments absorb much of visible light, but reflect more of the longer wavelengths of light (such as IR) (Proença, 2011; Bowyer et al., 2008; Daugman, 1994).
- Subjects have to position their eye within the camera's field of view and stand still as the iris photographs are acquired (Bowyer et al., 2008).
- The iris and pupil are considered to always present a circular shape (Sung et al., 2002).

In recent years it has been recognized that the path forward, regarding iris recognition, is the development of algorithms that can work independently of such conditions, in order to achieve ***robust*** (i.e. accurate even with noisy images) and ***unconstrained*** (i.e. accurate for several sets of acquisition conditions: distance, movement, illumination, etc.) iris recognition and, in this way, become a real-world applicable method (Ross, 2010; Proença, 2010). This paradigm shift lead to the rise of new trends in the research of iris recognition:

1. **Using visible wavelength (VW) light instead of NIR:** Current recognition systems require high illumination levels, to maximize the signal-to-noise ratio in the sensor and capture enough iris features with sufficient contrast. However if acquisition of iris images is pretended to work with longer distances and for moving individuals, significantly higher f-numbers and very short exposure times would be needed. Both these features require high levels of light intensity, which, in the case of NIR, could be hazardous to the eye, as its instinctive responses (aversion, blinking or pupil contraction) are not affected by NIR wavelengths. The use of VW light finds none of these constraints, and is, therefore, the current trend for iris image acquisition and database creation (iris databases will be discussed in section 3.5). However one main concern is strongly connected with the use of VW images: noise artifacts are more common and spectral reflectance is more prone to happen in such images. Figure 3.7 shows an example of both NIR and VW illumination effect on iris image qualities (Proença, 2010).

2. **Processing non-ideal irises:** Lots of factors may affect iris images and challenge the robustness of proposed algorithms. Some of these factors are motion blur, camera diffusion, out-of-focus imaging, occlusion from eyelids and eyelashes, off-axis gaze, specular reflections, poor contrast or natural luminosity (Ross, 2010). In the iris database sections some of these factors will be discussed with more detail. Attempts to process these less ideal features have been reported. Abhyankar et al. (Abhyankar et al., 2005) used repositioning of bi-orthogonal wavelet network (BWN) to compensate for off-angle iris images, with excellent results for angle offset values below 50°. Du et al. (Du et al., 2004) tested various methods of iris signature comparison for images with only partial zones of the iris available, with 90% accuracy rate for 40% occluded iris. Sung et al. (Sung et al., 2002) use eye corner detection to compensate the non-circularity induced in the iris shape by gaze direction.

Figure 3.7: Comparison between the typical appearance of (a) NIR iris images and (b) VW iris images (Proença, 2010).

3. **Active contour models:** instead of relying on rigid geometric models, many attempts have been made to develop models whose shape is deformable and adjustable to certain features of the iris image. Arvacheh (Arvacheh, 2006) uses an altered version of the Daugman integro-differential operator, which works by maximizing the external forces associated with the points of a contour, in small angular intervals, to detect the nearcircular contour of the pupil and use it as the beginning point for an iterative external force minimization process to detect the limbic boundary; Daugman (Daugman, 2007) suggests the use of Fourier series coefficients to actively detect iris contours; Ross et al. present an active contour-base method using a simple thresholding method, helped by 2D median filtering, to segment the pupil, and then use a geodesic active contour (GAC) approach to estimate the limbic boundary (Shah and Ross, 2009).

4. **Eyelid and eyelash model fitting:** Eyelids and eyelashes occluding the iris region are noise factors that degrade the performance of iris recognition. If they are incorrectly classified as the iris region, the false iris pattern information will increase, decreasing the recognition rate. Masek (Masek, 2003) proposed a post-segmentation step to separate iris and eyelid by horizontal lines (Figure 3.8). The linear Hough transform is used to detect the eyelid boundaries, and the intersection of these lines with the segmented iris contour will define the horizontal line. One of the main problems with this approach is that some information of the iris might be lost when such a coarse approach is applied. Kang and Park (Kang and Park, 2007) took a computationally more complex approach, by using the parabolic Hough Transform lowering the chance of missing iris zones, when compared to Masek's work.

5. **Performance Improvement:** In order to improve the computational speed and the resulting performance of iris recognition systems, some works have taken into consideration the development of faster algorithms. Liu et al. (Liu et al., 2005) base themselves in Masek's

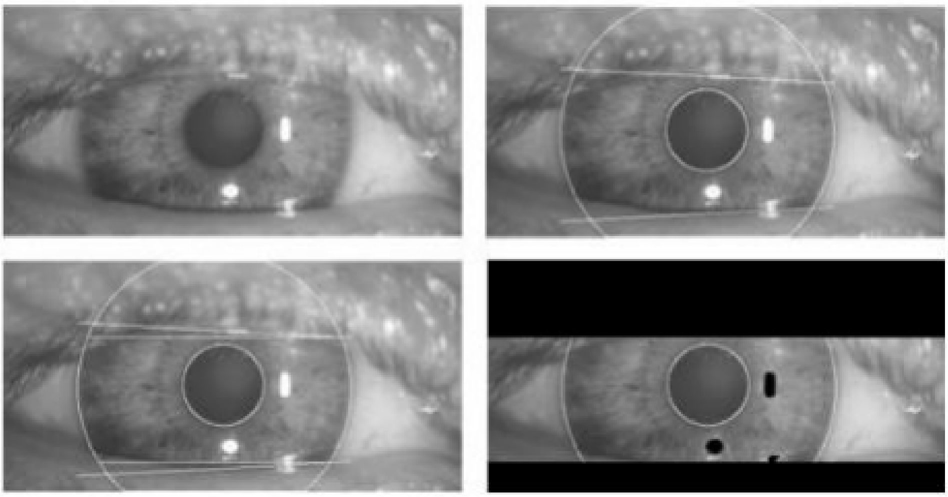

Figure 3.8: Application example of Masek's eyelid boundary detection via linear Hough transform (Masek, 2003).

work (Masek, 2003) with the Canny edge detector and the CHT and suggest some optimization steps, such as switching the border detection order (from limbic–pupillary to pupillary–limbic) because the iris/pupil contour normally presents higher contrast than the iris/sclera contour. This claim is highly dependent on the nature of the images, but, as seen on Figure 3.7 it seems to be a valid claim when working with NIR images. Some other suggested optimization steps are the reduction of edge pixels (restricting the number of high intensity edge candidates, generally associated with the reflections observed in the pupil), and the reduction of calculations in the Hough transform for eyelid detection, namely by reducing the range of possible values for the Hough transform parameters.

6. **Multiscale for iris image pre-processing and pattern analysis:** Because of their intrinsic characteristics, limbic and pupillary boundaries are found in zones of the image that correspond to local maxima of image gradient. However, due to the existence of noisy areas of the image, locating specific maxima is not an easy job. Smoothing operators provide an interesting weapon for noise removal, but their use is limited by the need of manually defining their scale: small smoothing kernels don't affect the global information of the image but might also not remove all the noise, while larger kernels will certainly remove the unintended noise, but might also remove information of interest. Taking this problem into consideration, some tools for multiscale analysis, like the wavelet transform, started to gain some importance in pre-processing of iris images or analysis of different texture levels. Edges of higher significance are more likely to be preserved by the wavelet transform across the scales. Edges of lower significance are more likely to disappear when the scale increases (Figure 3.9). Some works using multiscale analysis are (Nabti and Bouridane, 2008; Lu and Lu, 2008; Sanchez-Avila et al., 2002; Abhyankar and Schuckers, 2009).

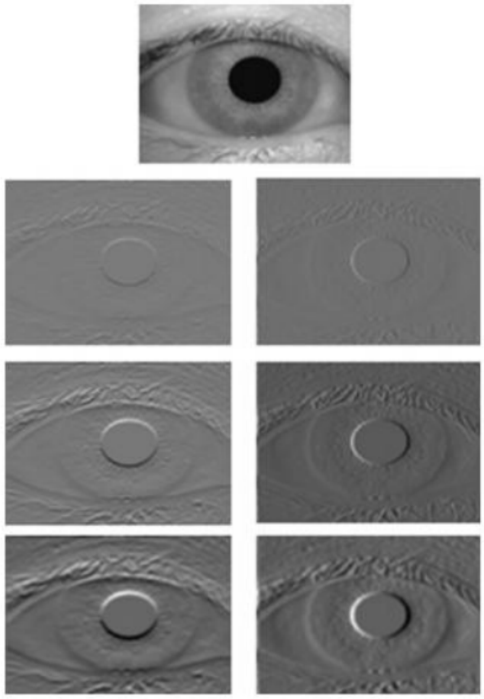

Figure 3.9: Example of multiscale approach for iris contour enhancement (Nabti and Bouridane, 2008).

3.5 Iris databases

Several free public databases are made available online for the testing of iris recognition algorithms. In this section the most commonly used databases are described, specifically the quality of the images, the different classes of images and the various kinds of noise factors that were considered. All these factors weighted the choice of the best database for the development of unconstrained iris recognition algortihms.

3.5.1 BATH database

The University of Bath iris image database (Figure 3.10) is a constantly growing database currently composed of over 16000 iris images taken from 800 eyes of 400 subjects. A series of acquisition and post-processing constraints assure good image quality with the main sources of noise being only obstruction by eyelids and eyelashes. For these reason this database in not very appropriate for the development of iris recognition algorithms under unconstrained settings.

3.5.2 CASIA database

Apart from being the oldest iris database, this is clearly the most known and widely used by the majority of the researchers. CASIA iris image database (Figure 3.11) includes 756 iris images from 108 eyes, captured in two distinct sessions. Similarly to the BATH database, described above, its

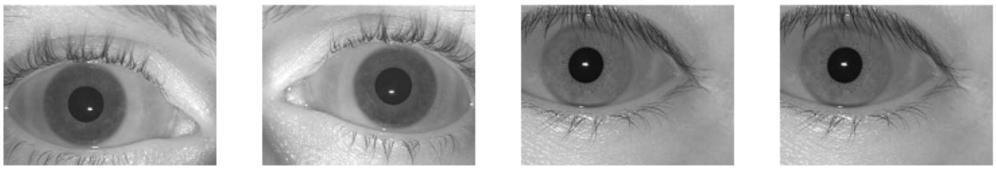

Figure 3.10: BATH database image examples (BATH, 2004).

images were captured under highly constrained capturing conditions, yielding very homogeneous characteristics and their noise factors are exclusively related with iris obstructions by eyelids and eyelashes. The images were also filled, in the pupil regions, with black pixels, which some authors used to facilitate the segmentation task. This way, the CASIA database cannot be considered to develop algorithms to be used under unconstrained environments.

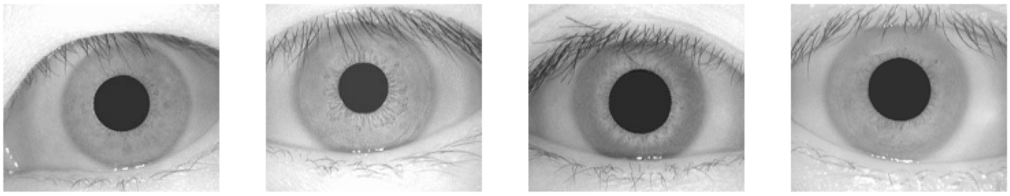

Figure 3.11: CASIA database image examples (CASIA, 2004).

3.5.3 ICE database

The Iris Challenge Evaluation (ICE) is a contest designed to measure the accuracy of iris recognition algorithms and is comprised of 2954 images (Figure 3.12), with a variable number of images per subject. Quality was the main concern in the creation of this database. Therefore, the noise factors that the ICE database contains are mainly related with iris obstructions and poorly focused images. Another drawback with this database is that it was only made available for researchers and entities that showed interest in participating in the competition (Proença, 2007).

Figure 3.12: ICE database image examples (ICE, 2006).

3.5.4 WVU database

The West Virginia University developed an iris image database (Figure 3.13) comprised of 1852 images from 380 different eyes. Images were captured in less constraining acquisition conditions and, due to this, incorporate several types of noise, such as iris obstructions, poorly focused and off-angle images. However, few iris images present significant specular and lighting reflections, which are believed to be the most common type of noises in images acquired under natural light.

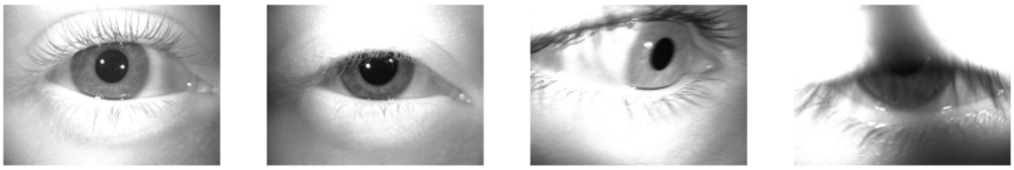

Figure 3.13: WVU database image examples (A. Ross and Schuckers).

3.5.5 UBIRISv2 database

The UBIRISv2 database is comprised of 1877 images collected from 241 subjects within the University of Beira Interior in two distinct sessions and constitutes the world's largest public and free iris database for biometric purposes. Acquisition conditions were unconstrained with several classes of noise factors characterized in several of the images that comprise this database. These factors are listed below and depicted in Figure 3.14:

- Iris obstruction by eyelids
- Iris obstruction by eyelashes
- Lightning reflections
- Specular reflections
- Poor focus
- Partially captured iris
- Out-of-image iris
- Off-angle iris
- Motion blurred images

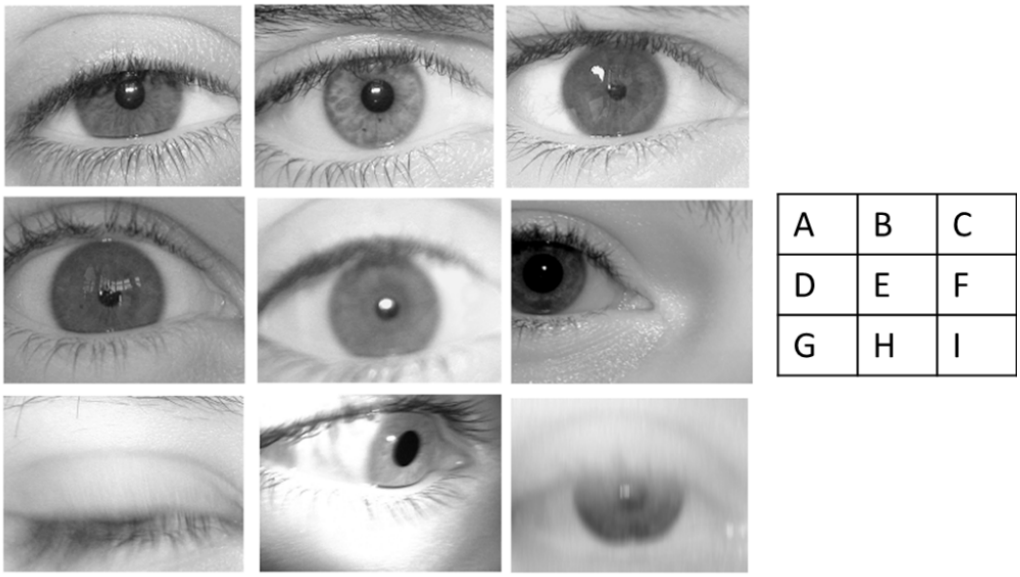

Figure 3.14: Types of noise found in UBIRIS database: (A) Eyelid obstruction; (B) Eyelash obstruction; (C) Lighting reflections; (D) Specular reflections; (E) Poor focus; (F) Partial iris images; (G) Out-of-image iris; (H) Off-angle iris; (I) Motion blurred image (Proença et al., 2010).

3.6 Proposed work motivation

The proposed work was motivated by all the limitation presented in the previous sections, regarding both algorithms and databases. Where algorithms are concerned the goal is the development of an algorithm that doesn't rely on the fact that the iris and the pupil are perfectly circular, and doesn't require complex acquisition systems (IR illumination, user collaboration or proximity, etc.) for iris images. This second objective seems to be overcome by using the UBIRISv2 database. However, as will be referred in further sections, it is proposed that the images from the UBIRISv2 database don't present enough information so as to allow the evaluation of feature extraction and matching algorithms, reducing its utility to the evaluation of segmentation and noise detection. With that in mind a new iris image database was created to allow both the evaluation of segmentation and recognition of the proposed algorithm.

Chapter 4

Proposed work: VCMI database and developed algorithm

4.1 Introduction

In this chapter the proposed algorithm is presented in two main sections: Section 4.3.1 presents the proposed segmentation algorithm, as well as some insight into some algorithms that inspired it; Section 4.4 gives some insight of the SURF feature extractor as well as its application for iris recognition. Additionaly the newly created VCMI iris database is presented in detail as well as the motivation behind its creation.

4.2 VCMI database

images are depicted in Figure 4.1. A new iris database was created, in a partnership with two students from ESEIG (Escola Superior de Estudos Industriais e de Gestão), with the main goal of testing the applicability of the developed algorithms, when working with images acquired with mobile devices.
For example, anyone could use bioemtric login in a smartphone to manage a bank account, or simply to substitute the commonly used PIN numbers. With this in mind a new iris database was created, using a smartphone and a camera, whose specifications are presented in Table 4.1.

The images were acquired in uniform yet uncontrolled conditions, with constant illumination,

Table 4.1: Specifications of the devices and images for each of the tested databases.

	Database		
	UBIRISv2	**VCMI Smartphone**	**VCMI Camera**
Device	Canon EOS 5D	Nokia 5800	Panasonic DMC-FX3
Resolution (pixels)	300×400	3.2 Megapixel (2048×1536)	6 Megapixel (3032×2008)
Image Format	*.tiff	*.jpeg	*.jpeg

and a distance between user and camera of approximately 20-30cm. Only photos from the right eye were taken, exploring a series of eye orientations , such as looking to the camera, looking sideways, upwards and downwards, and with partially occluded eyes. 100 individuals were involved in the acquisition session, with 10 images per device being taken. For the evaluation of the proposed algorithm a subset of 100 images per device, from 25 randomly chosen individuals (4 per individual) was created. Examples of the obtained images are depicted in Figure 4.1.

It is interesting to note that the images acquired for the VCMI database were all acquired is compressed .jpeg format. It is not known if the compression affected the iris images such as to affect the recognition results presented in Section 5.3. This interesting observation might be the focus of future works: to develop a database of both compressed and uncompressed images and assess the possible nefarious effects of such process in iris recognition.
Careful observation of the images presented in Figure 4.1 show that the images obtained with the camera are seriously affected by reflections of the person taking the images. The extent of such noise is variable in size but, in some images, covers the entire iris region, affecting all the information present in such area. This fact should affect recognition results but, as will be seen in Section 5.3, the error rates obtained for such images are still a lot lower than the ones obtained with the UBIRISv2 images.

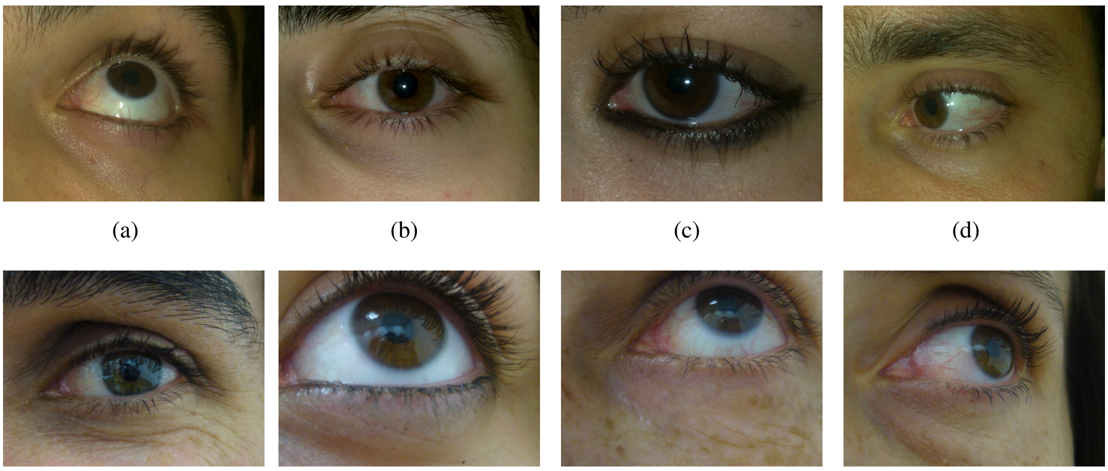

(a) (b) (c) (d) (e) (f) (g) (h)

Figure 4.1: Examples of images in the VCMI database. (a)-(d): Smartphone images and (e)-(h): Camera images

4.3 Segmentation

4.3.1 Simultaneous detection of iris center and limbic contour

Researchers are now paying more attention to the context to aid visual recognition processes. Context plays an important role in recognition by the human visual system, with many important visual recognition tasks critically relying on it. Central to the proposal in this work is the modeling of the mutual context of limbic contour and iris centre, so that each can facilitate the recognition of the other. When performed independently, both tasks are nontrivial since many other parts of the image may be falsely detected. However, the two tasks can benefit greatly from serving as context for each other.

4.3.1.1 Algorithm overview

The main steps of the proposed algorithm are systematized in Figure 4.2. The simultaneous detection of the iris centre and limbic contour was simplified by first over-detecting centre candidates, followed by a contour detection around each of them. The centre candidates are estimated by a method resembling the use of convergence index filters (Kobatake and Hashimoto, 1999). Next, a window centred in each candidate is converted into the polar domain and a shortest path algorithm is used to determine the best closed paths around the centre. Using combined data from the centre and respective contour, the best pair centre/contour is selected.

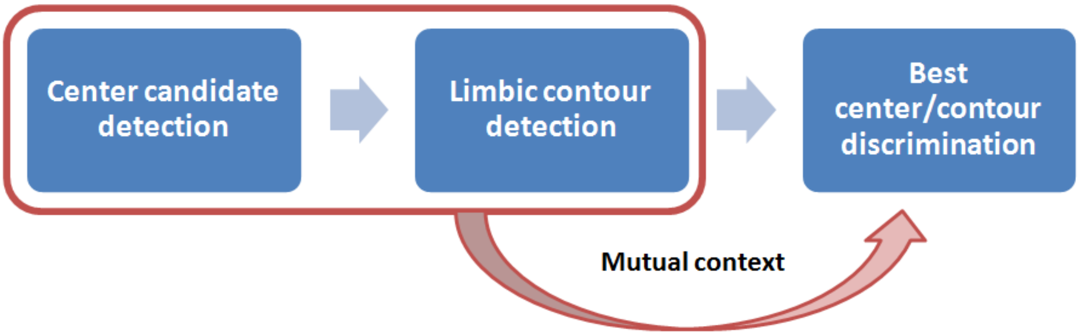

Figure 4.2: Flowchart of the proposed iris segmentation algorithm.

Typical iris images present two very distinct regions: a high intensity region corresponding to the eye and the skin, and the iris region, at least *partially circular* and *lower in intensity*. These two sources of knowledge can be presented separately but are intrinsically connected. The fact that the iris is a darker region against a brighter background translates into a specific divergent gradient orientation from its centre. At the same time the limbic contour (iris outer edge) will present a high gradient magnitude as well as a closed shape. The approach taken in this work was that of detecting pairs of iris centre and limbic contour candidates that maximize a quality factor weighted by the afforementioned combined knowledge.

4.3.1.2 Convergence index filters

The convergence index filter for vector fields was proposed by Kobatake et al. in 1999 (Kobatake and Hashimoto, 1999) as an algorithm for detection of round objects in images, such as cancerous tumour masses in chest X-ray images. The idea proposed by Kobatake et al. seemed interesting for application in the proposed iris segmentation algorithm as the iris is, at least partially, a distinct round object in eye images.

To aid the comprehension of this algorithm one must first understand the notion of gradient vector field applied to images. Theoretically the gradient is a vector field that points in the direction of the greatest rate of increase of a scalar field (Hazewinkel, 2001). Working with images the gradient is a vector field that points from darker regions (of lower intensity) towards brighter regions (of higher intensity) (Gonzalez et al., 2007). With this in mind it is easy to deduct that in an image composed of a brighter circular region, surrounded by a darker background, the gradient orientation vector field will be as depicted in Figure 4.3.

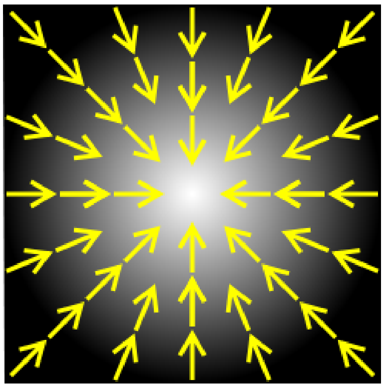

Figure 4.3: Gradient vector field orientation in a synthetic image.

The computation of the gradient orientation is achieved by first computing the horizontal and vertical components of the image gradient, G_x and G_y respectively. This can be achieved, as proposed by Kobatake, by using both orientations of Prewitt's kernel (Gonzalez et al., 2007):

$$\begin{pmatrix} -1 & 0 & 1 \\ -1 & 0 & 1 \\ -1 & 0 & 1 \end{pmatrix} \qquad \begin{pmatrix} -1 & -1 & -1 \\ 0 & 0 & 0 \\ 1 & 1 & 1 \end{pmatrix}$$

From the values of G_x and G_y the gradient magnitude and orientation can then be computed using Equations 4.1 and 4.2 respectively:

$$|g(x,y)| = \sqrt{{G_x}^2 + {G_y}^2} \tag{4.1}$$

$$\phi(x,y) = \arctan \frac{G_y}{G_x} \tag{4.2}$$

The theoretical basis behind Kobatake's algorithm was to compute, for each point in an image, a value, called *convergence index*, that measured how strongly the gradient vectors around a given point pointed towards it. A circular region of radius R, centered on each point of interest, $P = (x,y)$, was considered, as schematized in Figure 4.4. Considering an arbitrary point $Q \rightarrow (k,l)$ in R, the convergence index for point P will be obtained by computing the cosine of the angle $\theta(k,l)$

between the line $\overline{PQ}$ and the gradient orientation vector in Q, $g(k,l)$. The output of the convergence index filter, $C(i,j)$ at point P is given by taking the average convergence index of all points Q in R, considering the image as a discrete set of points. Formally the convergence index filter on point $P \rightarrow (x,y)$ is given by Equation 4.3:

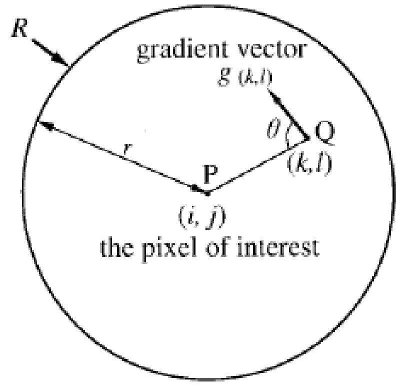

Figure 4.4: Region of interest for convergence index filter computation, as proposed by Kobatake in (Kobatake and Hashimoto, 1999).

$$C(i,j) = \frac{1}{M} \sum_{(k,l) \in R} \cos(\theta(k,l)) \tag{4.3}$$

The output of a convergence index (or COIN) filter is always between -1 and $+1$, with maximum value $+1$ corresponding to all the gradient vectors in R pointing towards P.

For the developed algorithm the idea behind COIN filters was applied to detected a set of iris center candidates, from the knowledge that the iris is a region of low intensity against a brighter background composed by the sclerotic region of the eye and the surrounding skin.

4.3.1.3 Iris center candidate detection

Iris centre candidates are detected using a template matching step between the gradient orientation of an iris image, exemplified in Fig. 4.5(b), and the template presented in Figure 4.5(a). This template fits the gradient orientation vector field observed in dark regions against bright backgrounds.

By computing the cross-correlation, c_{corr}, between the template and gradient orientation vector fields, a measure of the gradient divergence in each point can be achieved. The cross-correlation is obtained as described in Equation 4.4:

$$c_{corr} = (f * g)[\mathbf{n}] \stackrel{def}{=} \sum_{\mathbf{m}} f^*[\mathbf{m}] g[\mathbf{n}+\mathbf{m}] \tag{4.4}$$

where f^* and g represent the gradient orientation vector field and the template vector field, respectively.

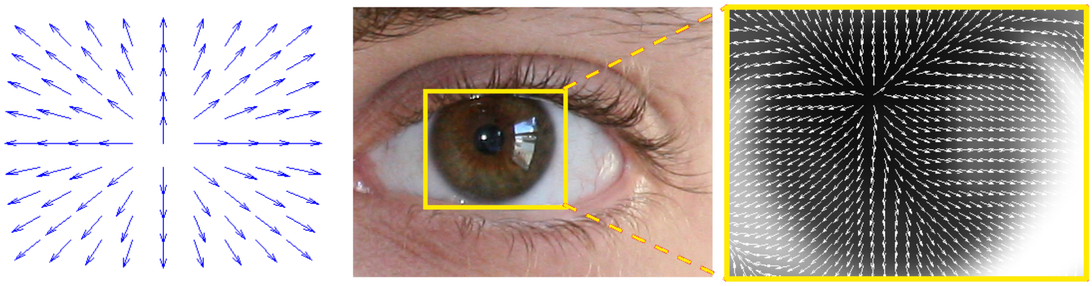

(a) (b)

Figure 4.5: The iris centre detection is based on two vector fields: a) Template vector field and b) Gradient orientation vector field. Note how the orientation around the iris centre fits the orientation template.

The resulting correlation values for each point can be represented as an image such as exemplified in Figure 4.6(a). The center candidates are chosen as the local maxima of cross-correlation, above a manually-tuned threshold, t_h. The local maxima are the set of points P_loc which, presenting a value above t_h, are higher than every neighboring pixel in a square window with size l. With this approach we significantly reduce the number of center candidates. For example, Figure 4.7, the direct application of the threshold would yield N candidates, while the local maxima detection reduces such number to one single point. The template matching step will, thus, yield a set of N iris center candidates. In the proposed work the variables t_h and l assumed the values 0.85 and 41 respectively, considering that all the images were resized to 300×400 and that the t_h value is normalized with respect to the maximum cross-correlation value obtained.

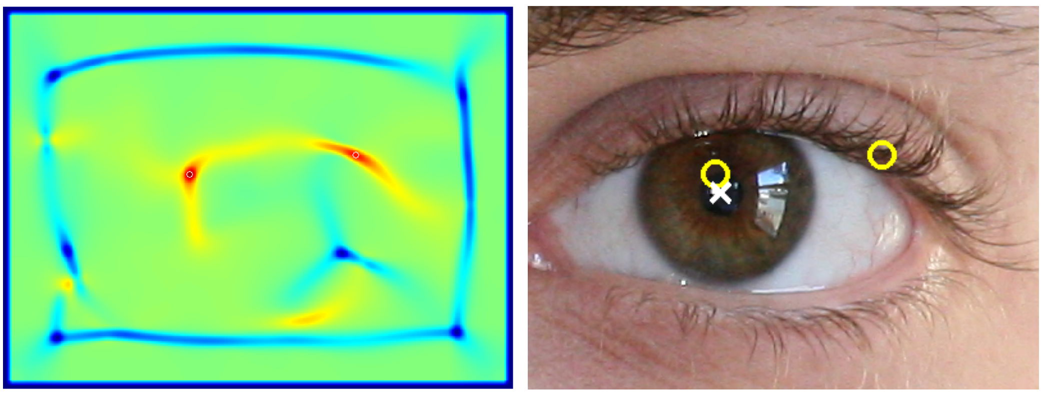

(a) (b)

Figure 4.6: Iris centre candidate detection: a) Cross-correlation result and b) Local maxima of cross-correlation (yellow circles) are the iris centre candidates. The white cross represents the real centre, manually annotated.

Since in the proposed method for limbic boundary detection the image grid is considered as a graph with pixels as nodes and edges connecting neighbouring pixels, we start by introducing

(a) (b) (c)

Figure 4.7: Local maxima computation: a) Original cross-correlation results (zoom to region of local maxima) b) pixels with intensity above threshold $th = 0.85$ c) Local maxima above threshold $th = 0.85$.

some graph concepts.

A *graph* $G = (V, A)$ is composed of two sets V and A. V is the set of nodes, and A the set of arcs (p, q), $p, q \in V$. The graph is *weighted* if a weight $w(p, q)$ is associated to each arc. The weight of each arc, $w(p, q)$, is a function of pixels values and pixels relative positions. A path from vertex (pixel) v_1 to vertex (pixel) v_n is a list of unique vertices $v_1, v_2, \ldots, v_n$, with v_i and v_{i+1} corresponding to neighbour pixels. The total cost of a path is the sum of each arc weight in the path $\sum_{i=2}^{n} w(v_{i-1}, v_i)$.

A path from a source vertex v to a target vertex u is said to be the *shortest path* if its total cost is minimum among all v-to-u paths. The distance between a source vertex v and a target vertex u on a graph, $d(v, u)$, is the total cost of the shortest path between v and u.

A path from a source vertex v to a sub-graph Ω is said to be the shortest path between v and Ω if its total cost is minimum among all v-to-$u \in \Omega$ paths. The distance from a node v to a sub-graph Ω, $d(v, \Omega)$, is the total cost of the shortest path between v and Ω:

$$d(v, \Omega) = \min_{u \in \Omega} d(v, u). \tag{4.5}$$

A path from a sub-graph Ω_1 to a sub-graph Ω_2 is said to be the shortest path between Ω_1 and Ω_2 if its total cost is minimum among all $v \in \Omega_1$-to-$u \in \Omega_2$ paths. The distance from a sub-graph Ω_1 to a sub-graph Ω_2, $d(\Omega_1, \Omega_2)$, is the total cost of the shortest path between Ω_1 and Ω_2:

$$d(\Omega_1, \Omega_2) = \min_{v \in \Omega_1, u \in \Omega_2} d(v, u). \tag{4.6}$$

4.3.1.4 Limbic contour as shortest closed path

Intuitively, limbic boundary appears as a closed contour in the image, enclosing the iris centre, and over pixels with a strong transition in the grey-level values. Assuming that paths through pixels with high gradient are preferred over paths through low gradient pixels, the limbic contour can then be found among the shortest closed paths enclosing the iris centre candidate. A difficulty with searching for the shortest closed path enclosing a given point C (shortest in the sense of minimizing the cost of the path) is that small paths, collapsing in the point C, are naturally favoured. We overcome that difficulty by working on polar coordinates. We assume that the origin of the coordinates is the candidate iris centre.

A circular window centred in each candidate is transformed to polar coordinates, as depicted in Figure 4.8. A closed path in the original Cartesian coordinates is transformed into a path from left to right margins in the window in polar coordinates, starting and ending in the same row of the transformed window.

Note that the main assumptions are a) the candidate centre lies within the true limbic contour; b) the limbic contour constitutes a closed path over pixels of strong gradient. The limbic contour is not necessarily circular and the candidate centre does not need to match the true iris centre for a correct contour detection.

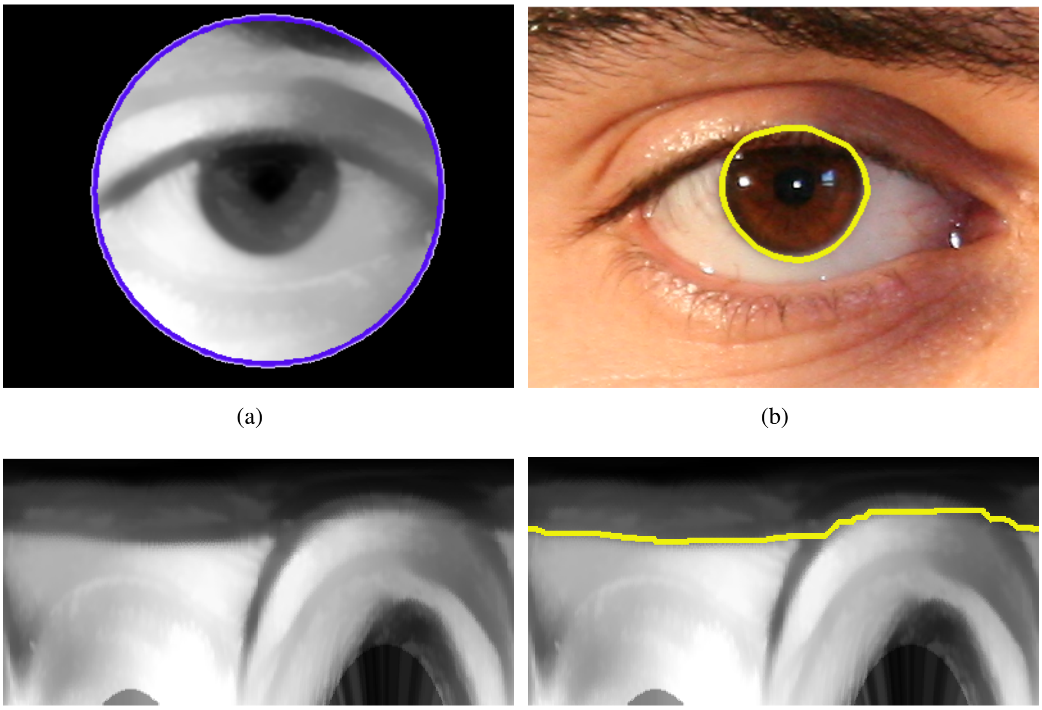

(a) (b)

(c) (d)

Figure 4.8: a) Circular window in original cartesian coordinates for polar transformation; b) Closed path in cartesian coordinates. c) Window after polar transformation. The origin is the top-left corner, the horizontal axis represents the angle, from 0 to 360 degrees, and the vertical axis the radius. d) Easily observable high gradient path, corresponding to the circular closed path of b).

4.3.1.5 Computation of the Shortest Closed Path

In spite of the efficiency of the computation of the shortest path between the whole left and right margins, or between two pre-defined points in the margins, or between one of the margins and a pre-defined point in the other margin, the search for the shortest path between the left and right margins with the constraint that the path should start and end in the same row seems to increase the complexity of the procedure. As typical, optimisation with constraints is more difficult than without.

Had one been interested in the simple shortest path between the left and right margin and the computation would be very efficiently performed using dynamic programming. Assuming the simplifying assumption that the vertical paths do not zigzag back and forth, up and down, in the transformed image, the search may be restricted among connected paths containing one, and only one, pixel in each column between the two end-columns.

Formally, let I be an $N_1 \times N_2$ window (after polar coordinate transform) with N_1 columns and N_2 rows ($N_1 = 360$ and $N_2 = 175$ in the proposed work); define an admissible path to be:

$$\mathbf{s} = \{(x, y(x))\}_{x=1}^{N_1}, \text{ s.t. } \forall x \ |y(x) - y(x-1)| \leq 1,$$

where y is a mapping $y : [1, \cdots, N_1] \rightarrow [1, \cdots, N_2]$. That is, an admissible path is an 8-connected path of pixels in the image from left to right, containing one, and only one, pixel in each column of the image.

The first step is to traverse the image from the second column to the last column and compute the cumulative minimum cost C for each entry (i, j):

$$C(i,j) = \min \begin{cases} C(i-1, j-1) & + \quad w(p_{i-1,j-1}; p_{i,j}) \\ C(i-1, j) & + \quad w(p_{i-1,j}; p_{i,j}) \\ C(i-1, j+1) & + \quad w(p_{i-1,j+1}; p_{i,j}) \end{cases},$$

where $w(p_{i,j}; p_{l,m})$ represents the weight of the edge incident with pixels at positions (i, j) and (l, m). At the end of this process,

$$\min_{j \in \{1, \cdots, N_2\}} C(N_1, j)$$

indicates the end of the minimal connected path. Hence, in the second step, one backtrack from this minimum entry on C to find the optimal path.

Note that this procedure gives not only the shortest path between the left and right margins but also yields the shortest path between any point in the right margin and the whole left margin: for any point (N_1, j) in the right margin, $C(N_1, j)$ indicates the cost of the shortest path between (N_1, j) and the whole left margin, see Figure 4.9. Finally, it should be clear how to change the initial conditions of the above procedure to yield the shortest path between two pre-defined points in the opposite margins.

Unfortunately, the computation of the shortest path constrained to start and end in the same row (corresponding to closed contours in the original window) does not seem amenable to such an

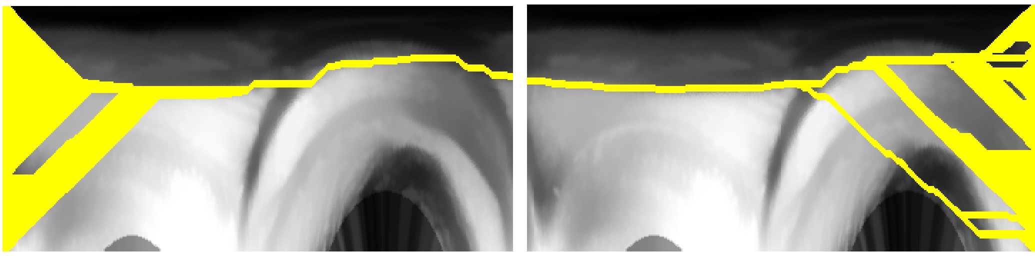

(a) (b)

Figure 4.9: Example of shortest path starting point detection. (a) shows all paths from the left margin to the right margin and (b) all the paths from the right margin to the left margin. As is observable all paths converge to a set of convergence points (in this case this set is composed by a single point), which serve as start/end points for a set of closed contours.

efficient procedure. The brute force solution of computing the shortest path between the i-point in the left margin and the i-point in the right margin, for $i = 1 \cdots N_2$, and taking the minimum, is not compatible with requirements of near real-time in our application.

Noting that if j and ℓ are two distinct points in the right margin, then the shortest paths between each of these points and the whole left margin do not intersect, it is trivial to conclude that there is at least one point m in the right margin for which the shortest path between m and the whole left margin starts also at row m. Note that the paths correspond to closed paths in the original window in cartesian coordinates (not necessarily including the shortest one). Similarly, interchanging the role of the left and right margin, it is possible to obtain at least one point n in the left margin for which the shortest path to the whole right margin is closed. By computing all the paths from the left to the right margin (and vice-versa), a set of k closed contours is obtained for each centre candidate. The procedure is illustrated in Figure 4.9.

4.3.1.6 Design of the Weight Function

The weight of an edge in the graph is a function of the values of the incident nodes (pixels). We start by computing the derivative in the radial direction (centred in the iris candidate position) in the original space, using a 3-point numerical differentiation (Secant), as defined in Eq. (4.7).

$$G_\theta(r) = \frac{I(r+h) - I(r-h)}{2h}, with h = 1 \tag{4.7}$$

In the graph, to each edge incident with 4-neighbouring pixels correspond a weight determined by the derivative value of the two incident pixels, expressed as an exponential law, presented in Eq. (4.8).

$$f(g) = f_\ell + (f_h - f_\ell)\,\frac{\exp(\beta\,(255-g)) - 1}{\exp(\beta\,255) - 1} \tag{4.8}$$

In this function $f_\ell, f_h, \beta \in \Re$ and g is the minimum of the derivative computed on the two incident pixels. For 8-neighbour pixels the weight was set to $\sqrt{2}$ times that value. The parameters

f_ℓ and f_h were fixed at $f_\ell = 2$ and $f_h = 32$; β was experimentally tuned using a grid search method, yielding $\beta = 0.0208$.

4.3.2 Best center/contour pair discrimination

From the previously described steps a set of centre/contour candidate pairs (Cp) is built. The joint decision for the centre and contour is taken to maximize the joint probability of the individual parts. In here, we assume that the joint probability is a monotonous function of the product of individual measures of quality, combined in an overall quality factor, Q. The discrimination between candidates is performed by choosing the pair with the highest Q. The quality factor is given by:

$$Q(Cp) = \frac{\mu(\Delta C) \cdot \rho_p}{(1 - S(C))}$$

where $\mu(\Delta C)$ is the mean derivative alongside the contour, ρ_p is the cross-correlation value of the centre candidate, and S is the shape factor of the contour (with perimeter P and area A), given by:

$$S(C) = \frac{P^2}{4\pi \cdot A}$$

The center/contour pair with the highest quality factor was chosen as the limbic contour. A high quality factor assured that the chosen pair presented a high cross-correlation value in its center candidates, a high mean gradient alongside its contour and an at least partial circular shape. This way the centre/contour pair is selected based on an optimal combination of these three factors. An example of two candidate pairs and their respective quality factor values is presented in Figure 4.10.

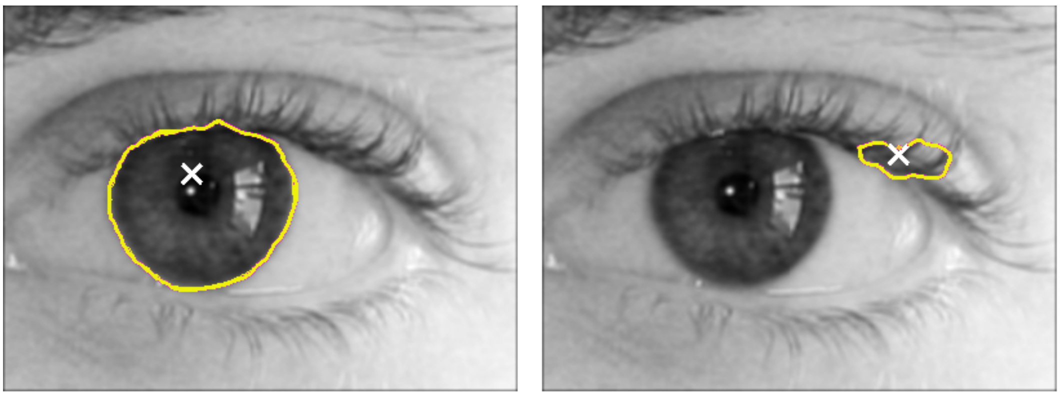

Q = 0.1337 **Q=0.0274**

Figure 4.10: Examples of the quality factor values, Q, for the two centre/contour candidates of a given image.

4.3.3 Pupillary contour and normalization

As it was referred, when presenting the pioneer works on iris recognition (Section 3.2), normalization of the segmented iris regions is an important step, in order to overcome size diferences between different iris images, as well as distinct contraction states of the pupil, by transforming the image into a *fixed size* polar image. This step was indispensible because such differences in iris image nature would affect the performance of the feature extraction and matching algorithms. However, in recent years, a series of algorithms have been developed that focus on the detection of scale invariant features in certain points of interest in the image:

- Scale Invariant Feature Transform - *SIFT* (Lowe, 1999)
- Speeded Up Robust Features - *SURF* (Bay et al., 2006)
- Gradient Location and Orientation Histogram - *GLOH* (Mikolajczyk and Schmid, 2005)
- Histogram of Oriented Gradients - *HOG* (Zhu et al., 2006)
- Local Energy based Shape Histogram - *LESH* (Sarfraz and Hellwich, 2008)
- Local Descriptor for Dense Wide-Baseline Stereo Matching - *DAISY* (Tola et al., 2010)

With such algorithms, objects can be described by certain features of specific points of interest, in a way that is independent of scale, illumination and rotation. In the proposed work, SURF (Bay et al., 2006), which will be described in detail in the next section, was used as the feature extraction algorithm. Normalization becomes less indispensible with SURF because points of interest can be extracted without the need for scale normalization and image transformation into the polar domain. By eliminating the need for a normalization step, the segmentation of the pupillary contour is also dispensable. The segmentation of the pupil in traditional methods aimed to compensate different pupil sizes, depending on its contraction state, allowing a normalization step that resulted in iris signatures with the same size, regardless of the pupillary dilation. With no need for normalization it was chosen *not to perform pupillary segmentation* as well. Another factor that also weighted in this choice was the fact that unconstrained settings in image acquisition yielded oftimes images where the distinction between iris and pupil, either due to heavily pigmented iris or reflection noise, was not considerable. Figure 4.11 shows some examples of this effect. Some attempts were made, using the UBIRISv2 database, at executing pupillary segmentation with an approach similar to the one proposed for the limbic contour. However, due to the problems outlined above the results were far from satisfactory, especially when images from different databases were tested. With this in mind, the pupillary segmentation process was discarded.

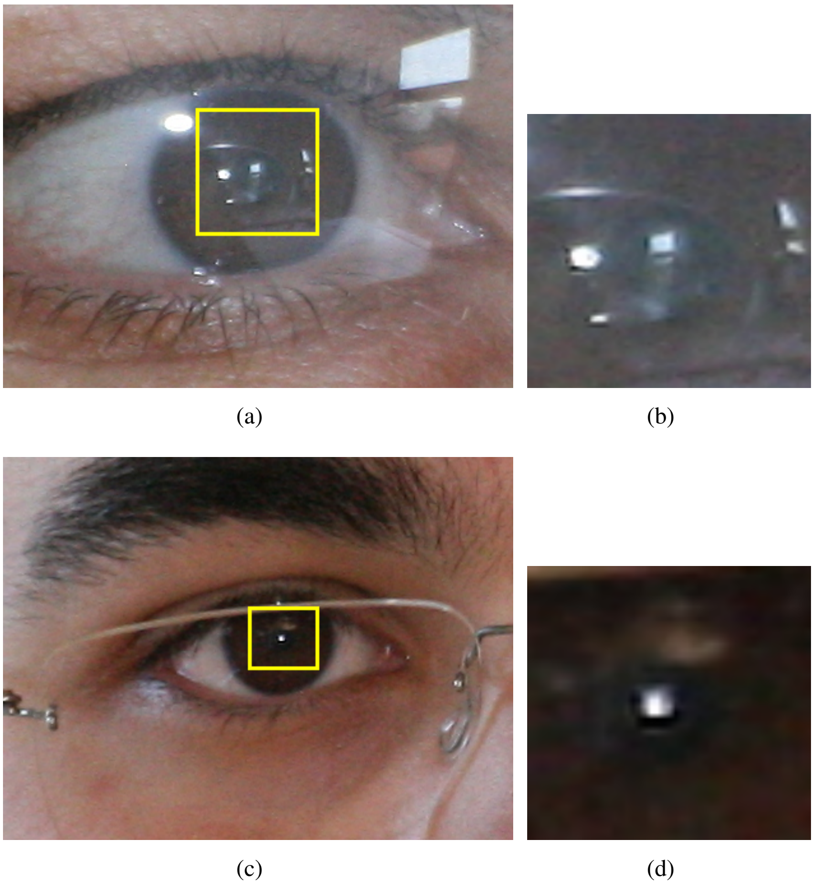

Figure 4.11: Example of iris images, acquired under unconstrained settings, where the contrast between pupil and iris is significantly low. Images like these backed the idea that pupillary segmentation in such images is not as straightforward as limbic contour segmentation.

4.4 Recognition

4.4.1 Speeded Up Robust Features

Typically, the search for image point correspondences can be divided into three main steps. A set of *interest points* are selected at distinctive landmarks in the image, such as corners, blobs, or T-junctions. These points all present the key property of repeatability, that is, the reliability of a detector for finding the same physical interest points under different viewing conditions. The neighbourhood of every interest point is then represented by a *feature vector*. This *descriptor* has to be distinctive and at the same time robust to noise, detection, displacements and geometric deformations. Finally, the descriptor vectors are *matched* between different images. The matching is based on a distance between the vectors, like the Mahalanobis or Euclidean distance. The dimension of the descriptor has a direct impact on the computing time of such process, with lower dimensions being more desirable for fast interest point matching. However, lower dimensional feature vectors are in general less distinctive than their high-dimensional counterparts (Bay et al., 2008).

In 2006, Bay et al. proposed a methodology denominated *Speeded Up Robust Features* or *SURF* that aimed to achieve a computationally fast, with little or no effect on performance, detector and descriptor algorithm that achieved scale and rotation invariance (Bay et al., 2006). As these are two factors that are difficult to control while acquiring iris images, as depicted in Figure 4.12, the SURF algorithm seemed an interesting alternative to attempt recognition between two iris signatures.

(a) (b)

Figure 4.12: Example of two iris images from the same person but with distinct scale and rotation values.

4.4.1.1 Point of interest selection

The most widely used detector probably is the Harris corner detector (Harris, 1988), proposed back in 1988. However, due to Harris corners not being scale-invariant, Lindeberg (Lindeberg, 1998) proposed the detection of interest points in an image, each with their own characteristic scale, experimenting both the determinant and the trace of the Hessian matrix. On the original SURF paper (Bay et al., 2006) the authors analyze a series of variants of interest point detection algorithms based on Harris corners and features of the Hessian matrix and achieved two main conclusions:

- Hessian-based detectors are more stable and repeatable than their Harris-based counterparts.
- Using the determinant of the Hessian matrix rather than its trace seems advantageous.

With this in mind they proposed a point of interest detection based on the determinant of the Hessian matrix. However, rather than using a different measure for selecting the location and the scale, they relied on the determinant of the Hessian matrix $H(X,\sigma)$, for both. For each point $X = (x,y)$ in an image I, the Hessian matrix in X at scale σ is defined as:

$$H = \begin{pmatrix} L_{xx}(X,\sigma) & L_{xy}(X,\sigma) \\ L_{xy}(X,\sigma) & L_{yy}(X,\sigma) \end{pmatrix}$$

where $L_{xx}(X,\sigma)$ is the convolution of the Gaussian box filters second order derivative $\frac{\delta^2}{\delta x^2} g(\sigma)$ with the image I in point X and similarly for $L_{xy}(X,\sigma)$ and $L_{yy}(X,\sigma)$. The use of box filters instead of normal 2D Gaussians, as depicted in Figure 4.13, arises as a result of the need for discretization and crop of Gaussians for their practical application, which can bring about problems such as aliasing as the resulting images are sub-sampled, with the possibility of new structures appearing when working at lower resolutions (higher σ values). Box filters are easy to implement using integral images and allow fast computation time because of the simple weights applied in the rectangular regions presented in Figure 4.13.

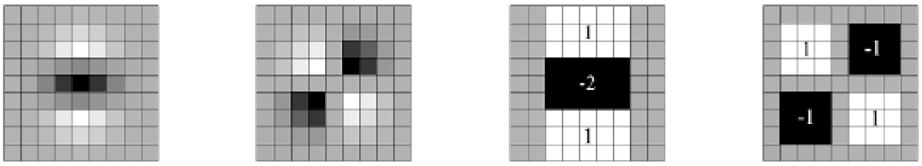

Figure 4.13: From left to right: Discretized and cropped Gaussian second order partial derivatives in y-direction and xy-direction, and proposed approximations by box filters. The grey regions are zero (Bay et al., 2006).

The 9×9 box filters in Fig 4.13 are approximations for Gaussian second order derivatives with $\sigma = 1.2$ and represent the lowest proposed scale (i.e. highest spatial resolution). The results of the convolutions with the proposed box filter approximations of second derivative Gaussians are denoted D_{xx}, D_{yy}, and D_{xy} and the calculation of the Hessian matrix determinant can be easily accomplished using these three values:

$$det(H(X,\sigma)) = D_{xx} \cdot D_{yy} - (D_{xy})^2$$

To work with variable scales algorithms generally work with *image pyramids*: each scale will yield a result and such results will be stacked in a three-dimensional array. In the SURF point detector the images are repeatedly smoothed with Gaussian box filters and subsequently sub-sampled (i.e. the σ value is doubled and the filter size is adapted) in order to achieve a new scale value for a new level of the image pyramid. The interest points are detected as local maxima in the image pyramid array, using a non-maximum suppresion algorithm in a 3 x 3 x 3 neighbourood.

4.4.1.2 SURF point descriptors

Each point of interest, detected as a local maximum of the Hessian determinant image pyramid, is associated to a feature vector, extracted from its neighborhood, also known as the *descriptor*. To create these descriptors an *orientation* value is computed for each point of interest, based on

Gaussian weighted Haar wavelet response in both x and y directions in a circular region around the interest point. The size of the region is dependent on the scale value, s, of the interest point. The orientation of each point of interest is computed by plotting the horizontal against the vertical components of the Haar wavelet responses, and calculating the maximum response sum in a sliding window like the one depicted in Figure 4.14. By assigning an orientation value to each point of interest, SURF descriptors may achieve orientation invariance.

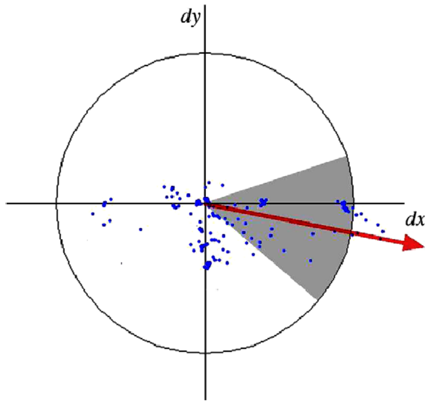

Figure 4.14: Orientation assignment of each point of interest: a sliding orientation window of size $\pi/3$ detects the dominant orientation of the Gaussian weighted Haar wavelet responses at every sample point within a circular neighbourhood around the interest point (Bay et al., 2006).

After the orientation value is computed, a square region, centered on the point of interest, oriented along its orientation direction and with side length proportional to the scale value is defined. This region is divided into smaller 4×4 square sub-regions, and for each sub-region the Haar wavelet responses along x and y are computed for 5 equally separated sample points. The x and y directions are considered with respect to the orientation direction of the point of interest. Each sub-region will yield as final feature vector a set of 4 values: $(\sum d_x, \sum d_y, \sum |d_x|, \sum |d_y|)$, where d_x and d_y are the horizontal and vertical components of the Haar wavelet response in each of the sample points of the sub-region. The final feature vector for each point of interest will, therefore, be composed by the 16 sets of 4 features, yielding a 64 features descriptor for each point of interest. This process is depicted in Figure 4.15.

4.4.1.3 Matching of points of interest from two images

The matching between points of interest in two different images is simply made by calculating the point in one of the images that presents the minimum distance (Euclidean or Mahalanobis, for example) to a point in the other image. Even though this seems trivial, one simple addition is made to the obtained 64D descriptors for each point. As it can be seen in Figure 4.16 two similarly shaped regions should not be considered a match. One simple way to distinguish between them without the need to compute distance measures is to compare the trace of the Hessian matrix

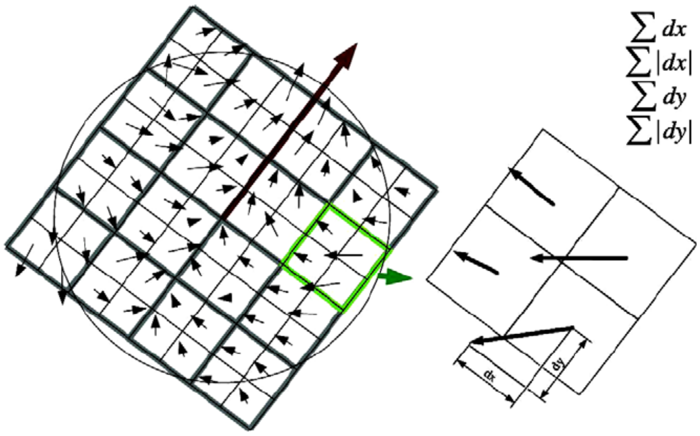

Figure 4.15: Descriptor building process for each point of interest: an oriented quadratic grid of 4×4 square sub-regions is laid over the interest point (left). For each square, the wavelet responses are computed from 5×5 equally separated sample points (for illustrative purposes, only 2×2 sub-divisions are shown). For each field, the Haar wavelet responses in both direction, d_x and d_y, and their respective modulus, $|d_x|$ and $|d_y|$, were computed relatively to the orientation of the grid (right). (Bay et al., 2008).

for each point of interest, and using the sign of this result as a first matching step, without extra additional computing cost (Bay et al., 2008).

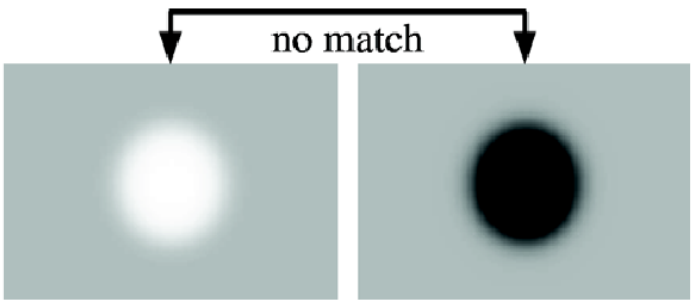

Figure 4.16: If the contrast between two interest points is different (dark on light background vs. light on dark background), the candidate is not considered a valid match (Bay et al., 2008).

4.4.2 Iris mask estimation

4.4.2.1 Mask effect on SURF point of interest detection

To compare two iris images one most only consider the region corresponding to the iris. The segmentation algorithm presented in previous sections achieved this goal by detecting the limbic contour, that separates the iris from the sclerotic region of the eye. However, the SURF algorithm searches all the points in a given image for points of interest. Without iris segmentation, SURF would detect a lot of keypoints with no interest for recognition. For example in Figure 4.17 it can be observed that the SURF point detector yields a significant set of points of interest. Without any conditioning to the keypoint localization the regions of the eyebrows and the shadows, that naturally arise from varying illumination conditions, will present gradient characteristics that fit the SURF point detector targets. With this in mind it is important to create a *binary iris mask image* to restrict the possible locations of the detected keypoints. Figure 4.17 shows the difference between the detected keypoints with and without the application of the mask image.

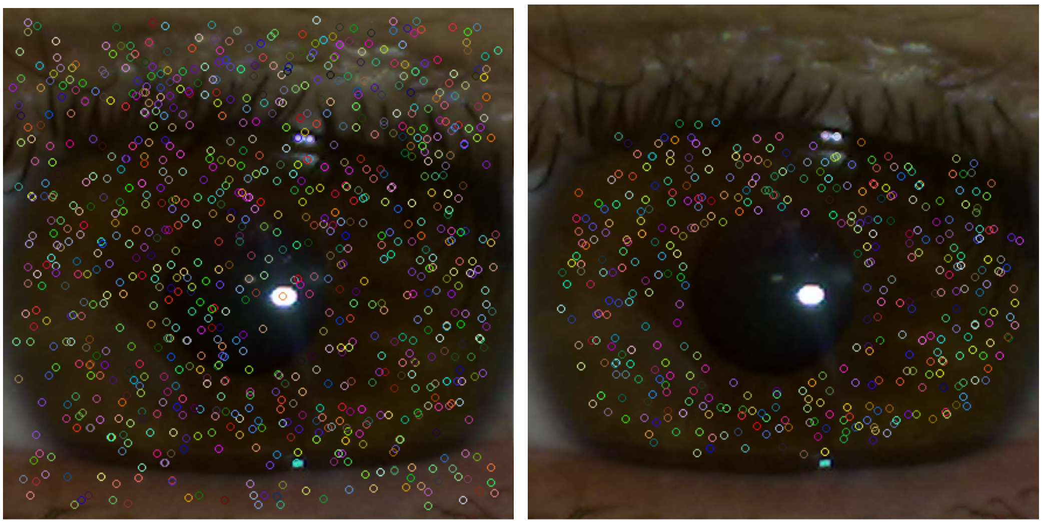

(a) (b)

Figure 4.17: Results of the SURF keypoint detector for: a) the full iris image and b) the masked iris image.

4.4.2.2 Mask estimation

To estimate such mask a set of parameters was considered:

- The region surrounded by the detected limbic contour, L_{ch};
- A circular region, centred on C_i and with radius $r_i/3$ to serve as an approximation of the pupil region.

The first item of the list presented above is simple to understand: after detecting the limbic contour with the proposed segmentation algorithm, the region of interest (ROI) corresponding to the iris will be the area surrounded by such contour. However, inside this region one can also find the pupil. Even though the pupil is generally a region of very uniform low intensity, some features of such region might introduce noise on the SURF algorithm. For example, if no removal of the pupil was performed, the segments of the pupillary contour that present higher contrast will probably be detected by the SURF point of interest detector. The problem with such points is that, as refered above, pupillary segmentation is not a trivial step when working with images acquired under unconstrained settings. To overcome such problem an *approximation of the puppilary region* was performed in order to assure that no points of interest in the puppilary contour were considered for matching.

It is known that illumination affects the size of the pupil (Taptagaporn and Saito, 1990). This is a difficult problem to overcome, as it implies that no direct relation exists between the size of the iris and the pupil. With this in mind, a choice had to be made whether to consider always the worst cas scenario, that is, consider that the pupil is always fully dilated and work only with the points of the iris farthest away from the center, or risk a smaller pupil region with the tradeoff of a larger region of the iris. Regardless of the choice, the rationale followed to create an approximation of the pupil was to compute a circular region centred on the same point as the iris, C_i, and with a radius proportional to the radius of the iris, r_i. The proportionality constant used in this work was $1/3$.

4.4.3 Matching

The SURF algorithm finds, for each point of interest in an image I_1 , the best match with all the points in another image I_2 . The best match is the point of interest in I_2 that presents lowest distance to the point of interest of I_1. To perform matching between two iris images the best matches from the pair of images are considered. By considering only the best matches, iris belonging to the same person will present lower mean errors than iris from different persons. Using the iris mask defined by the segmentation process only points of interest arising from iris patterns are considered. Figure 4.18 exemplifies the point of interest matching for two images of the same individual and for two images of distinct individuals. After the matching of the best pairs of points of interest from two images is carried out, the mean matching error from each pair is computed. The recognition is carried out by using as a similarity measure the mean error from the 10% best matches from a pair of images, that lie inside the iris mask defined by segmentation. This approach may seem too simple but presented some interesting results (see Section 5). However such approach does not take in account the position of the points of interest, or other geometric measurements. Using geometric information (such as relative point position, convex hull area and perimeter, etc.) might be an interesting approach to achieve more accurate recognition using SURF point of interest descriptors.

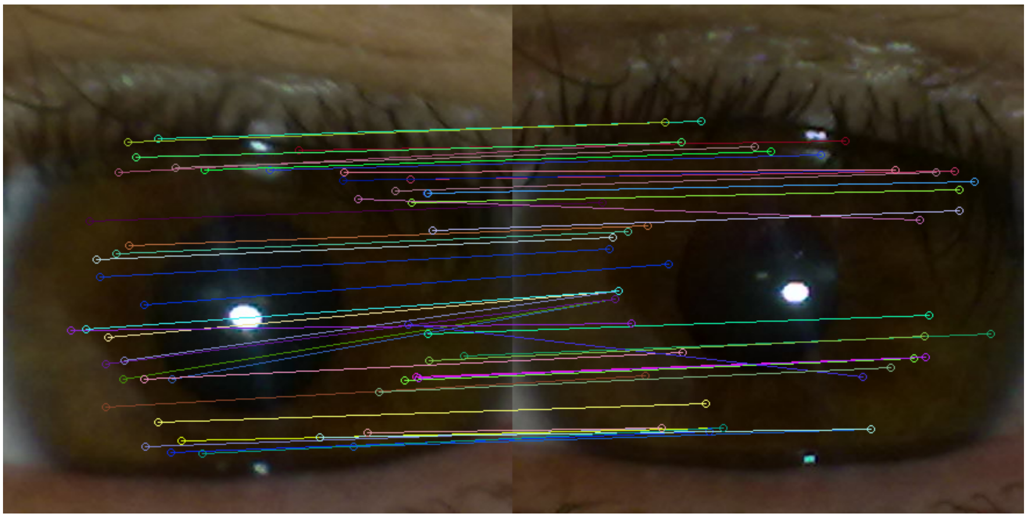

(a)

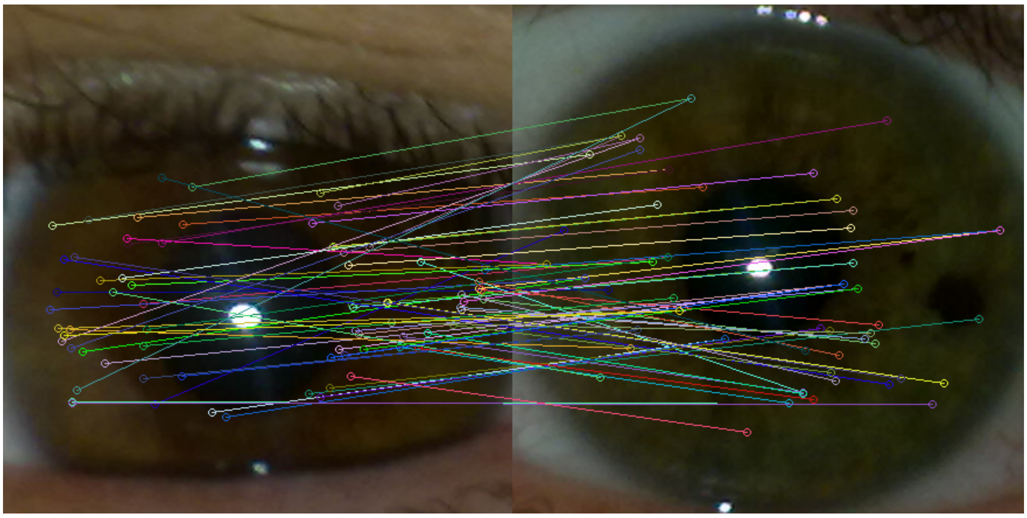

(b)

Figure 4.18: Results of matching for: a) images from the same individuals and b) image from distinct individuals.

Chapter 5

Results and Discussion

In this chapter the main results of the proposed algorithm are presented. The results are divided, as the description of the algorithm, in two main sections: Section 5.2 presents the segmentation errors and Section 5.3 the recognition results with all the tested databases.

5.1 UBIRISv2 database

The proposed algorithm was evaluated, initially, in the UBIRISv2 database Proença et al. (2010). Images in UBIRISv2 were captured under non-constrained conditions (at-a-distance, on-the-move and on the visible wavelength), with corresponding realistic noise factors. In Figure 5.1 some of these noise factors (reflections, occlusions, pigmentation, etc.) are exemplified. A subset of the original database composed by 100 images from 20 distinct individuals was created. All 100 images were manually annotated so as to allow the evaluation of the obtained results. All individuals and respective images were chosen randomly.

5.2 Segmentation

5.2.1 Colour channel selection

In order to apply the proposed algorithm the RGB images from the UBIRISv2 database were converted to a single colour channel. Literature suggests that the red channel is the optimal colour channel for iris segmentation. Behind this statement is the fact that the iris presents more sensitivity to infra-red wavelength. With this in mind working with the red channel should convey the most useful information for iris segmentation (Tan et al., 2010). Such information led to the choice of the red channel as the input for the segmentation algorithm and all the results presented, regardless of the database, were obtained using that channel.


(a)

(b)

(c)

(d)

(e)

(f)

(g)

(h)

Figure 5.1: Examples image classes in the UBIRISv2.0 database: a) Heavily occluded; b) Heavily pigmented; c) Glasses occlusion; d)Reflection occlusion; e) Off-angle; f) Rotated eye; g) Black subjects and h) Normal.

5.2.2 Iris centre

The iris centre detection accuracy was measured as the Euclidean distance between the centre of the automatically selected centre/contour pair and the manually marked iris centre. In order to report errors, independently of the distance of the camera to the individual, the distance was normalised by the mean radius of the manually annotated limbic contour. As the iris is not always exactly circular, the point from which the gradient diverges is not always the real iris centre. This observation helps to understand why the iris centre errors, summarized in Table 5.1 are not lower. However it can be noted that the mean error is significantly lower than the radius of the iris, and the automatically detected centre lied always inside the iris region. This is the most significant observation, since it is a pre-requisite for a successful limbic contour detection. With this in mind the obtained results show that the proposed algorithm accomplishes its main goal, with errors significantly lower than the iris radius, regardless of the tested database.

Table 5.1: Main results obtained with the proposed algorithm.

		Database		
		UBIRISv2	**VCMI Smartphone**	**VCMI Camera**
Centre	**Distance (%)**	14.56	11.27	14.81
Contour	**Mean error (%)**	5.72	8.18	12.07
	Hausdorff distance (%)	14.64	21.93	30.21
	Mean iris radius (pixels)	65.1	31.4	37.8

The presented results show that the images acquired with the camera give the worst segmentation results. However these results are affected by a common cause for high segmentation errors:

as depicted in Figure 5.2 some of the off-angle images (where the iris is totally shifted to one side of the sclera) present the iris/sclera contrast only one of the sides of the image. This confuses the shortest path algorithm: instead of sticking to the limbic contour the shortest path will diverge to a region of higher contrast, like the skin and the eyelashes, thus causing segmentation errors such as the ones exemplified in Figure 5.2. Such error could be possibly overcome by detecting the sclera before starting the segmentation of the limbic contour and using such information to better limit the segmentation process. It must be noted that all the images, regardless of the database, were resized to approximately 300×400 to speed up the segmentation process. The original images were then cropped (bounding box of the iris region), according to the region segmented as iris, for the recognition process.

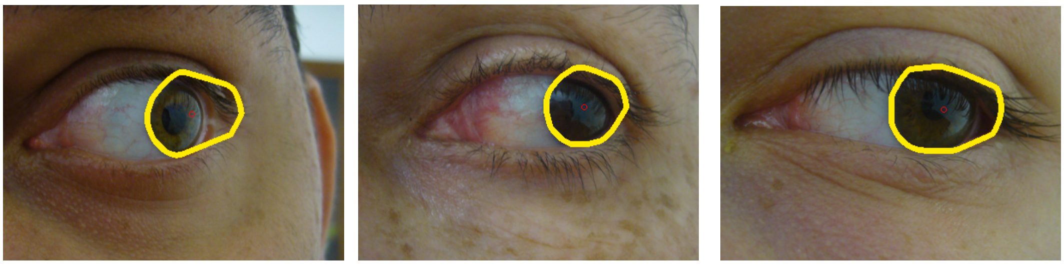

(a) (b) (c)

Figure 5.2: Segmentation errors with off-angle images. As it can be observed the existence of a well defined sclera region on only one of the sides of the iris affects greatly the limbic contour on the side where the contrast is reduced.

5.2.3 Limbic contour

The evaluation of the limbic contour was performed by computing the mean distance between each point of the detected contour and the closest point of the manually annotated contour. Besides the mean error, the Hausdorff distance between both the aforementioned contours was also calculated. The Hausdorff distance is defined as the "maximum distance of a set to the nearest point in the other set". Roughly speaking, it captures the maximum separation between the manual and the automatic contours. As with the centre error calculation, both distances were normalized with respect to the iris radius.

Some of the obtained results are depicted in Figures 5.3 and 5.4, for the UBIRISv2 and VCMI Smartphone databases respectively, alongside de manually annotated ground truth. It is observable that the most considerable errors are observed in the upper part of the eyes, near the eyelashes. This is easily explained as the eyelashes are generally dark regions that are easily mistaken with the iris, given that the cost function for the shortest path algorithm is based solely on gradient magnitude. However, these errors could be easily overcome by the application of an eyelid/eyelash detection algorithm like the ones proposed by Masek (2003) or Kang (Kang and Park, 2007). The UBIRISv2 database presented the best segmentation results. However none of the results obtained with the other database (VCMI Camera and VCMI Smartphone) can be considered negative, as the iris was localized (i.e. the correct center/contour pair was selected) for all the tested images, regardless of the database.

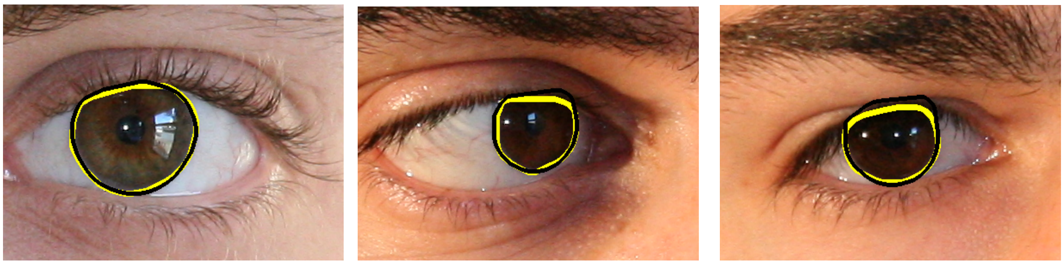

(a) (b) (c)

Figure 5.3: Contours obtained by the proposed algorithm on the UBIRISv2 database (black) and the manually annotated contours (yellow).

5.2.4 Centre/contour pair discrimination

The quality factor proved to be an excellent asset for discrimination of the best centre/contour pair, as is observed by the results summarized in Table 5.2. Some images present very high correlation values on other dark regions of the image, such as eyebrows or thicker eyelashes. Such areas also presented high gradient values and, thus, created the need for a third evaluation parameter. The shape factor gave higher weight to more circular shapes, such as the iris. The quality factor allowed zero miss detection of the best centre/contour pair. To prove the importance of mutual context information, all the images were re-tested with the assumption that the best centre/contour pair would always correspond to the highest cross-correlation value. With this new assumption a miss-detection ratio of 8% was obtained, for the UBIRISv2 database, thus confirming the importance of mutual context information. An example of the segmentation results with both approaches is depicted in Figure 5.5. With the VCMI database the importance of the quality factor was even more pronounced with miss-detection ratios of 14% and 11% obtained using the highest cross-correlation value (for VCMI smartphone and VCMI camera images respectively), and a zero miss-detection obtained through the calculation of the quality factor. Figure 5.6 shows an example of the quality factor discriminative power with an image from the VCMI smartphone database.

Table 5.2: Miss-detection results of the tested databases with and without the quality factor. Without the quality factor the best center/contour pair qas considered as the candidate with higher cross-correlation value.

	Database		
	UBIRISv2	**VCMI Smartphone**	**VCMI Camera**
Without Q (%)	8	14	11
With Q (%)	0	0	0

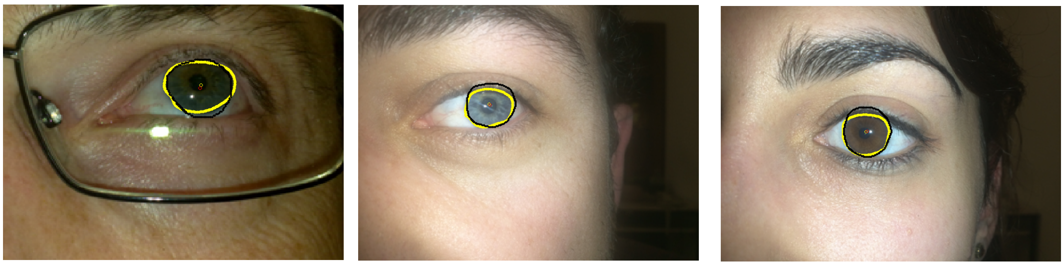

(a) (b) (c)

Figure 5.4: Contours obtained by the proposed algorithm on the VCMI smartphone database (black) and the manually annotated contours (yellow).

(a) (b)

Figure 5.5: Example of segmentation results with the discrimination by (a) proposed quality factor and (b) global maximum of cross-correlation as best centre.

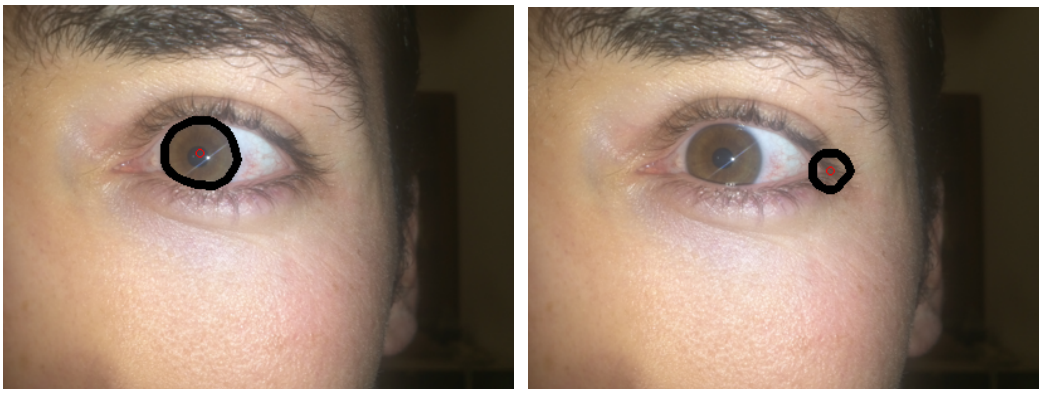

(a) (b)

Figure 5.6: Example of segmentation results with the discrimination by (a) proposed quality factor and (b) global maximum of cross-correlation as best centre on images from the VCMI database.

5.2.5 Comparative analysis with state-of-the-art algorithms

In 2008, Hugo Proenca and Luis Alexandre, from Universidade of Beira Interior (UBI), Portugal, promoted the NICE.I Contest (http://nice1.di.ubi.pt/). This contest aimed to "evaluate the robustness to noise of iris segmentation and noise detection algorithms, toward iris recognition systems within less constrained image capturing conditions, eventually to covert ones, in the near future". The NICE results represent the great majority of the already available segmentation results using the UBIRISv2 database. However the evaluation parameters of the aforementioned contest are based on two principles that significantly vary from our proposed approach:

1. The segmentation of the iris region of the eye was based both on the detection of the limbic and the pupillary contours. In our work we performed no segmentation of the pupillary contour, as we argue that performing recognition regardless of this step might prove as the path forward, as far as unconstrained iris recognition is concerned. The rationale behind such decision is based on the fact that the contrast between the pupil and the iris is very dependent on many factors (illumination, iris pigmentation, obstructions, etc.) thus creating a serious challenge as far as the development of robust segmentation algorithms is concerned.

2. The final segmentation results are evaluated as number of pixels correctly classified as iris. This description takes in consideration the detection of noisy areas (reflections or eyelashes for example) which surpasses the scope of the proposed work.

With these two points in mind it is obvious that a direct comparison with the NICE.I segmentation results is not possible.

5.2.6 Processing time

The proposed segmentation algorithm was developed in MATLAB r2011a and presented a mean processing time of 18.83 seconds. The algorithm was tested on a Pentium (R) Dual-Core T4200@ 2.00GHz, 3.00GB RAM memory Toshiba Satellite portable computer.

5.3 Recognition

The recognition results for the UBIRISv2 database and the VCMI images (smartphone and camera) are presented in Figure 5.7. On the left side of each subfigure is the ROC curve for the two sets of images and on the right side the FAR vs. FRR curves. As it can be seen a significantly lower equal error rate (5.56% and 9.35% vs. 39.2%) was obtained for both the VCMI image types.

Although a few works present better recognition results with the UBIRISv2 database (Santos and Hoyle, 2012; Tan et al., 2012; Wang et al., 2012), this results are still very modest when compared to the existent systems working under constrained settings, as refered by Bowyer in his review on recognition works using the UBIRISv2 database (Bowyer, 2012). The obtained results with the UBIRISv2 database seem to indicate that the proposed algorithm might not work, as it is developed at the moment, with images with as low resolution as the UBIRISv2 images. However a few observations can be made regarding the usability of such a database for the evaluation of recognition algorithms. Using the SURF points of interest detector all the images in the VCMI database presented, at least, 100 points of interest, while 18% of the UBIRISv2 images presented no points of interest inside the iris region. This observation may present a limitation to the use of point-of-interest descriptors for iris recognition, but the number of recent works following this rationale (Bakshi et al., 2012; Liu and Li, 2012; Bakshi, 2011) might point that using SURF for feature extraction is a valid approach. The simplistic way of similarity calculation between two images might account for the big error rates obtained for the UBIRISv2 images, and further work in this area might lead to interesting results.

For real life applications the smartphone images, as well as the images acquired with the camera, presented promising results to be applied in security applications. The feature extraction and matching step needs to be perfected and the real applicability of techniques like SURF needs to be assessed. Noise assessment in the iris masks and the development of a robust pupil segmentation algorithms are the two logic steps to follow the presented work.

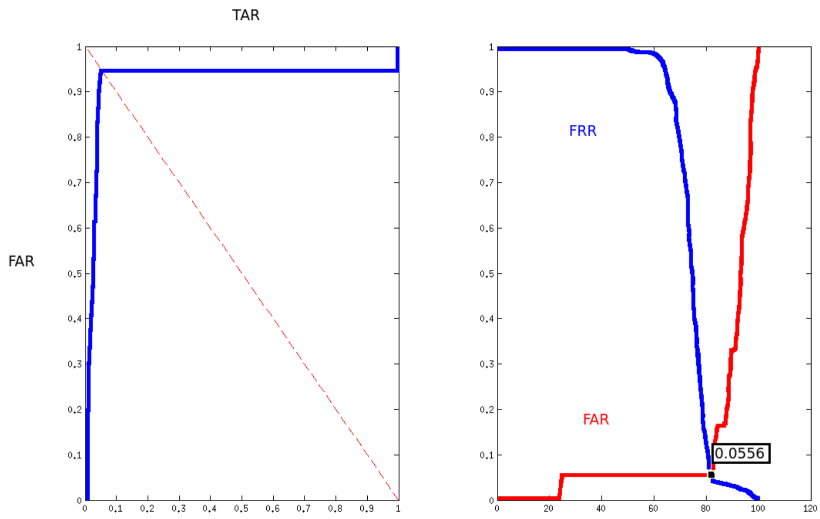

(a)

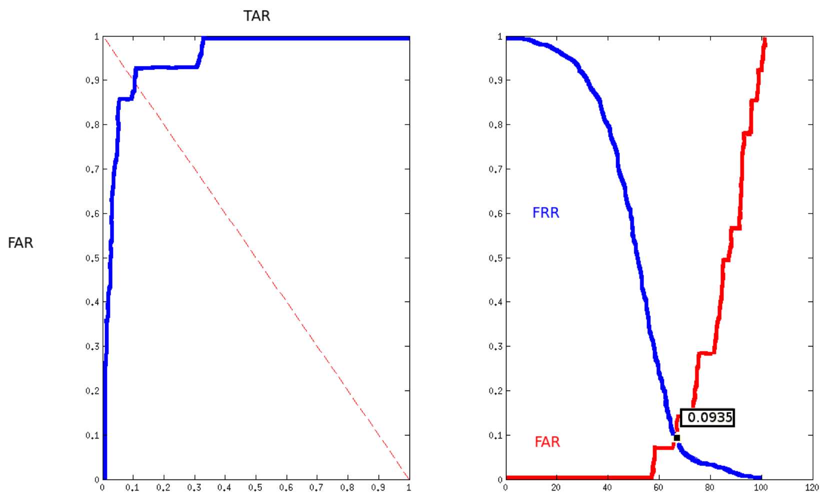

(b)

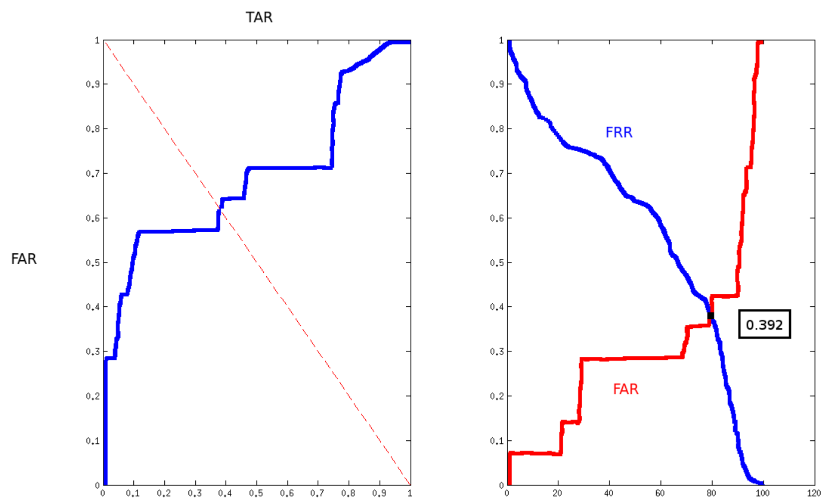

(c)

Figure 5.7: Recognition results, on the form of ROC curves and FAR vs FRR graphics, with: (a) VCMI smartphone images, (b) VCMI camera images and (c) UBIRISv2 database images.

Chapter 6

Conclusion

With the rising challenges in the unconstrained iris recognition field, regarding the use of images acquired under an unconstrained set of conditions, the development of new improved systems is gaining renewed interest. In the presented work a new rationale for iris segmentation, the first step in iris recognition, was presented.

The use of mutual information from gradient orientation for centre detection and gradient magnitude for contour detection presented good results, regardless of the chosen database, with zero miss-detection ratio of the best centre/contour pair. Future improvements on the segmentation algorithm should centre on the idea of improving the iris mask to help the recognition algorithm by either detecting zones of noise or attributing noise probabilities to each pixel and use such information when extracting the points of interest. SURF proved as an usefu alternative to the traditional Gabor based feature extraction methods by overcoming the need for pupillary segmentation (difficult in images acquired under unconstrained settings) and, thus, normalisation. The future work proposed for segmentation would improve the discrimination of points of interest, but testing new metrics (instead of just the mean matching error, as proposed) would also allow the improvement of the results presented in Chapter 5. With such metrics the algorithm could become less dependent in the resolution of the images, as observed by the results of the lower resolution UBIRISv2 images, and reach more interesting error rates. The VCMI database can also be perfected, by working with variable illumination conditions, distances between user and device, acquiring images from both eyes, testing different image formats and even acquire only partial regions of the iris.

Improving the robustness of the recognition algorithm and implementing it in a functional prototype is the near future goal for the present work.

References

L. Hornak A. Ross, S. Crihalmeanu and S. Schuckers. A centralized web-enabled multimodal biometric database. In *Proceedings Biometric Consortium Conference*.

A. Abhyankar and S. Schuckers. Iris quality assessment and bi-orthogonal wavelet based encoding for recognition. *Pattern Recognition*, 42(9):1878 – 1894, 2009.

A. Abhyankar, L. Hornak, and S. Schuckers. Off-angle iris recognition using bi-orthogonal wavelet network system. In *Fourth IEEE Workshop on Automatic Identification Advanced Technologies*, pages 239 – 244, 2005.

H. Ailisto, E. Vildjiounaite, M. Lindholm, S. Makela, and J. Peltola. Soft biometrics – combining body weight and fat measurements with fingerprint biometrics. *Pattern Recognition Letters*, 27 (5):325 – 334, 2006.

S. Angle, R. Bhagtani, and H. Chheda. Biometrics: a further echelon on security. 2005.

B. Arbab-Zavar and M. S. Nixon. On guided model-based analysis for ear biometrics. *Computer Vision and Image Understanding*, 115(4):487 – 502, 2011.

E. M. Arvacheh. A study of segmentation and normalization for iris recognition systems. Master's thesis, 2006.

S. Bakshi. Development of robust iris localization and impairment pruning schemes. Master's thesis, 2011.

S. Bakshi, S. Das, H. Mehrotra, and P.K. Sa. Score level fusion of sift and surf for iris. In *International Conference on Devices, Circuits and Systems*, pages 527 –531, march 2012.

D. Bala. Biometrics and information security. In *Proceedings of the 5th annual conference on Information security curriculum development*, InfoSecCD '08, pages 64–66, 2008.

J.R. Barnett, Sarah Miller, and Emma Pearce. Colour and art: A brief history of pigments. *Laser Technology*, 38(4):445–453, 2006.

N. Barzegar and M.S. Moin. A new approach for iris localization in iris recognition systems. In *Proceedings of the International Conference on Computer Systems and Applications (AICCSA2008)*, pages 516 –523, 2008.

BATH. University of bath iris image database, 2004. URL http://www.bath.ac.uk/elec-eng/pages/sipg/.

H. Bay, T. Tuytelaars, and L. Van Gool. Surf: Speeded up robust features. In Ales Leonardis, Horst Bischof, and Axel Pinz, editors, *Computer Vision*, volume 3951 of *Lecture Notes in Computer Science*, pages 404–417. Springer Berlin / Heidelberg, 2006.

H. Bay, A. Ess, T. Tuytelaars, and L. Van Gool. Speeded-up robust features (surf). *Computer Vision and Image Understanding*, 110(3):346 – 359, 2008.

Griaule Biometrics. *Types of Biometric Systems*, chapter 1. Griaule Biometrics, 2008.

Ruud Bolle and Sharath Pankanti. *Biometrics, Personal Identification in Networked Society: Personal Identification in Networked Society*. 1998.

K. W. Bowyer. The results of the nice.ii iris biometrics competition. *Pattern Recognition Letters*, 33(8):965 – 969, 2012.

K. W. Bowyer, K. Hollingsworth, and P. J. Flynn. Image understanding for iris biometrics: A survey. *Computer Vision and Image Understanding*, 110(2):281 – 307, 2008.

P. Buddharaju, I.T. Pavlidis, P. Tsiamyrtzis, and M. Bazakos. Physiology-based face recognition in the thermal infrared spectrum. *IEEE Transactions on Pattern Analysis and Machine Intelligence*, 29(4):613 –626, 2007.

CASIA. Casia iris image database., 2004. URL http://www.sinobiometrics.com.

C. Chang, J. Lee, Y. Su, S. H. Ping, and T. Tu. Using empirical mode decomposition for iris recognition. *Computer Standards and Interfaces*, 31(4):729 – 739, 2009. ISSN 0920-5489.

J. Chang and K. Fan. A new model for fingerprint classification by ridge distribution sequences. *Pattern Recognition*, 35(6):1209 – 1223, 2002.

R. Chen, X.R. Lin, and T.H. Ding. Iris segmentation for non-cooperative recognition systems. *Image Processing, IET*, 5(5):448 –456, 2011.

Y. Chen, M. Adjouadi, C. Han, J. Wang, A. Barreto, N. Rishe, and J. Andrian. A highly accurate and computationally efficient approach for unconstrained iris segmentation. *Image and Vision Computing*, 28(2):261 – 269, 2010.

J. G. Daugman. Biometric personal identification system based on iris analysis, 1994.

J.G. Daugman. High confidence visual recognition of persons by a test of statistical independence. *IEEE Transactions on Pattern Analysis and Machine Intelligence*, 15(11):1148 –1161, 1993.

J.G. Daugman. New methods in iris recognition. *IEEE Transactions on Systems, Man, and Cybernetics, Part B: Cybernetics,*, 37(5):1167 –1175, 2007.

A. de Santos Sierra, C. Sanchez Avila, G. B. del Pozo, and J. Guerra Casanova. Unconstrained and contactless hand geometry biometrics. *Sensors*, 11(11):10143–10164, 2011.

J. H. Doggart. Ocular signs in slit-lamp microscopy, 1949.

Y. Du, R. Ives, B. Bonney, and D. Etter. Analysis of partial iris recognition. In *SPIE Defense and Security Symposium*, 2004.

L. Flom and A. Safir. Iris recognition system, 1986.

D. Gabor. Theory of communication. part 1: The analysis of information. *Electrical Engineers - Part III: Radio and Communication Engineering, Journal of the Institution of*, 93(26):429 –441, 1946.

Z.J. Geng. Three-dimensional ear biometrics system and method, 2010.

R. C. Gonzalez, R. E. Woods, and S. L. Eddins. *Digital Image Processing Using MATLAB*. 2007.

H. Gray. *Gray's Anatomy*. Arcturus Publishing, 2010.

G. Guo and M.J. Jones. Iris extraction based on intensity gradient and texture difference. In *IEEE Workshop on Applications of Computer Vision (WACV 2008)*, pages 1 –6, 2008.

C. Harris. A combined corner and edge detector. *Proceedings of the Alvey Vision Conference*, 1988.

M. Hazewinkel. *Encyclopaedia of Mathematics*. Springer, 2001.

Z. He, T. Tan, Z. Sun, and X. Qiu. Toward accurate and fast iris segmentation for iris biometrics. *IEEE Transactions on Pattern Analysis and Machine Intelligence*, 31(9):1670 –1684, 2009.

N. Houhou, A. Lemkaddem, V. Duay, A. Alla, and J.P. Thiran. Shape prior based on statistical map for active contour segmentation. In *15th IEEE International Conference on Image Processing*, pages 2284 –2287, 2008.

A. V. Iannarelli. *Ear identification*. Paramount Pub Co., Fremont, California, 1989.

ICE. Iris challenge evaluation, 2006. URL http://iris.nist.gov/ICE/.

A. Jain, L. Hong, and S. Pankanti. Biometric identification. *Communications ACM*, 43(2):90–98, 2000.

A.K. Jain and Kumar A. *Biometrics of Next Generation: An Overview*, chapter 10. Springer, 2010.

A.K. Jain, A. Ross, and S. Prabhakar. An introduction to biometric recognition. *IEEE Transactions on Circuits and Systems for Video Technology*, 14(1):4 – 20, jan. 2004. ISSN 1051-8215.

A.K. Jain, A. Ross, and S. Pankanti. Biometrics: a tool for information security. *IEEE Transactions on Information Forensics and Security*, 1(2):125 – 143, 2006.

B. J. Kang and K. R. Park. A robust eyelash detection based on iris focus assessment. *Pattern Recognition Letters*, 28(13):1630–1639, 2007.

M. Kass, A. Witkin, and D. Terzopoulos. Snakes: Active contour models. *International Journal of Computer Vision*, 1(4):321–331, 1988.

H. Kobatake and S. Hashimoto. Convergence index filter for vector fields. *IEEE Transactions on Image Processing*, 8(8):1029 –1038, aug. 1999.

E. Krichen, S. Garcia-Salicetti, and B. Dorizzi. A new phase-correlation-based iris matching for degraded images. *IEEE Transactions on Systems, Man, and Cybernetics, Part B: Cybernetics*, 39(4):924 –934, 2009.

E. C. Lee, K. R. Park, and J. Kim. Fake iris detection by using purkinje image. In *Proceedings of the 2006 international conference on Advances in Biometrics*, ICB'06, pages 397–403. Springer-Verlag, 2006.

T. Lindeberg. Feature detection with automatic scale selection. *International Journal of Computer Vision*, 30:79–116, 1998.

X. Liu and P. Li. An iris recognition approach with sift descriptors. In De-Shuang Huang, Yong Gan, Phalguni Gupta, and M. Gromiha, editors, *Advanced Intelligent Computing Theories and Applications, with Aspects of Artificial Intelligence*, volume 6839 of *Lecture Notes in Computer Science*, pages 427–434. Springer Berlin / Heidelberg, 2012.

X. Liu, K.W. Bowyer, and P.J. Flynn. Experiments with an improved iris segmentation algorithm. In *Fourth IEEE Workshop on Automatic Identification Advanced Technologies*, pages 118 – 123, oct. 2005.

D.G. Lowe. Object recognition from local scale-invariant features. In *The Proceedings of the Seventh IEEE International Conference on Computer Vision*, volume 2, pages 1150 –1157 vol.2, 1999.

C. Lu and Z. Lu. Local feature extraction for iris recognition with automatic scale selection. *Image and Vision Computing*, 26(7):935 – 940, 2008.

L. Ma, T. Tan, Y. Wang, and D. Zhang. Local intensity variation analysis for iris recognition. *Pattern Recognition*, 37(6):1287 – 1298, 2004.

L. Masek. Recognition of human iris patterns for biometric identification. towards non-cooperative biometric iris recognition. In *Measurement*, 2003.

N. Mastali and J.I. Agbinya. Authentication of subjects and devices using biometrics and identity management systems for persuasive mobile computing: A survey paper. In *Fifth International Conference on Broadband and Biomedical Communications*, pages 1 –6, 2010.

K. Mikolajczyk and C. Schmid. A performance evaluation of local descriptors. *IEEE Transactions on Pattern Analysis and Machine Intelligence*, 27(10):1615 –1630, october 2005.

M. Nabti and A. Bouridane. An effective and fast iris recognition system based on a combined multiscale feature extraction technique. *Pattern Recognition*, 43(3):868 – 879, 2008.

L. Nanni and A. Lumini. A supervised method to discriminate between impostors and genuine in biometry. *Expert Systems with Applications*, 36(7):10401 – 10407, 2009.

H. Proença. Iris recognition: On the segmentation of degraded images acquired in the visible wavelength. *IEEE Transactions on Pattern Analysis and Machine Intelligence*, 32(8):1502–1516, 2010.

H. Proença. Non-cooperative iris recognition: Issues and trends. In *EUSIPCO 2011: 19th European Signal Processing Conference*, pages 2259 – 2263, 2011.

Hugo Proença. *Towards Non-Cooperative Biometric Iris Recognition*. PhD thesis, University of Beira Interior, Portugal, 2007.

Hugo Proença, S. Filipe, R. Santos, J. Oliveira, and L. A. Alexandre. The ubiris.v2: A database of visible wavelength iris images captured on-the-move and at-a-distance. *IEEE Transactions on Pattern Analysis and Machine Intelligence*, 32(8):1529 –1535, 2010.

J. Renaghan. Etched in stone. *Smithsonian Zoogoer*, 1997.

A. Ross. Iris recognition: The path forward. *Computer*, 43(2):30 –35, feb. 2010. ISSN 0018-9162.

K. Roy, P. Bhattacharya, C.Y. Suen, and J. You. Recognition of unideal iris images using region-based active contour model and game theory. In *17th IEEE International Conference on Image Processing*, pages 1705 –1708, 2010.

C. Sanchez-Avila, R. Sanchez-Reillo, and D. de Martin-Roche. Iris-based biometric recognition using dyadic wavelet transform. *Aerospace and Electronic Systems Magazine, IEEE*, 17(10):3 – 6, 2002.

G. Santos and E. Hoyle. A fusion approach to unconstrained iris recognition. *Pattern Recognition Letters*, 33(8):984 – 990, 2012.

M.S. Sarfraz and O. Hellwich. Head pose estimation in face recognition across pose scenario. In *International conference on computer vision theory and applications*, volume 1, pages 235–242, 2008.

A. Seal, M. Nasipuri, D. Bhattacharjee, and D.K. Basu. Minutiae based thermal face recognition using blood perfusion data. In *International Conference on Image Information Processing*, pages 1 –4, 2011.

R.R. Seeley, T.D. Stephens, and P. Tate. *Anatomy and Physiology*. McGraw-Hill, 2007.

S. Shah and A. Ross. Iris segmentation using geodesic active contours. *IEEE Transactions on Information Forensics and Security,*, 4(4):824 –836, 2009.

E. Sung, X. Chen, J. Zhu, and J. Yang. Towards non-cooperative iris recognition systems. In *7th International Conference on Control, Automation, Robotics and Vision*, volume 2, pages 990 – 995, 2002.

T. Tan, Z. He, and Z. Sun. Efficient and robust segmentation of noisy iris images for non-cooperative iris recognition. *Image and Vision Computing*, 28(2):223 – 230, 2010.

T. Tan, X. Zhang, Z. Sun, and H. Zhang. Noisy iris image matching by using multiple cues. *Pattern Recognition Letters*, 33(8):970 – 977, 2012.

S. Taptagaporn and S. Saito. How display polarity and lighting conditions affect the pupil size of vdt operators. *Ergonomics*, 33(2):201–208, 1990.

E. Tola, V. Lepetit, and P. Fua. Daisy: an Efficient Dense Descriptor Applied to Wide Baseline Stereo. volume 32, pages 815–830, May 2010.

M. Vatsa, R. Singh, and A. Noore. Improving iris recognition performance using segmentation, quality enhancement, match score fusion, and indexing. *IEEE Transactions on Systems, Man, and Cybernetics, Part B: Cybernetics,*, 38(4):1021 –1035, 2008.

T. Velho. Reconhecimento de íris em dispositivos moveis. Technical report, Universidade da Beira Interior, 2009.

Q. Wang, X. Zhang, M. Li, X. Dong, Q. Zhou, and Y. Yin. Adaboost and multi-orientation 2d gabor-based noisy iris recognition. *Pattern Recognition Letters*, 33(8):978 – 983, 2012.

R.P. Wildes. Iris recognition: an emerging biometric technology. *Proceedings of the IEEE*, 85(9): 1348 –1363, 1997.

Q. Zhu, M. Yeh, K. Cheng, and S. Avidan. Fast human detection using a cascade of histograms of oriented gradients. In *IEEE Computer Society Conference on Computer Vision and Pattern Recognition*, volume 2, pages 1491 – 1498, 2006.

J. Zuo and N.A. Schmid. On a methodology for robust segmentation of nonideal iris images. *IEEE Transactions on Systems, Man, and Cybernetics, Part B: Cybernetics,*, 40(3):703 –718, 2010.